

UNIVERSITÀ DEGLI STUDI DI PAVIA
FACOLTÀ DI INGEGNERIA
Dipartimento di Meccanica Strutturale

CAROTID ARTERY STENTING :
A COMPUTATIONAL SUPPORT
FOR PRE-OPERATIVE PLANNING.

by

Mauro Ferraro

Supervisor: PROF. FERDINANDO AURICCHIO

Co-supervisor: ENG. MICHELE CONTI

A Thesis submitted in Partial Fulfilment of the requirements
for the degree of Master in
Biomedical Engineering

Academic year
2010/2011

*Ai miei genitori per il supporto in questi anni, nonostante i protei e le
dispense sugli insetti facessero abbastanza schifo*

Aknowledgements

First of all, I want to thank my supervisor Prof. Ferdinando Auricchio for the complete support during this thesis work. I am especially grateful to Eng. Michele Conti, more a friend than a teacher definitely, for the support in the bad days and the laughs in the good ones. You're a great reasearcher and, this is more important, a great person. I would like to thank all the fellows who passed with me these wonderful days, I hope to keep in touch with all of you in the future. This aknowledgement should be obvious, but i want to thank my family for every single day they believed in me. Last but not least, i want to thank my girlfriend Maria Luisa because, day after day, she makes me a better man.

Abstract

I materiali a memoria di forma (SMA) rappresentano una classe di materiali metallici dalle particolari proprietà meccaniche. La loro caratteristica principale è quella di essere in grado di recuperare una forma preimpostata per effetto del semplice cambiamento di temperatura o dello stato di sollecitazione applicato. Queste peculiari proprietà, unite ad altre caratteristiche quali un'ottima resistenza a fatica o l'elevata biocompatibilità, hanno reso questi materiali protagonisti in vari campi di applicazioni in ambito biomedico. In particolare è possibile trovare una massiccia presenza degli SMA nei dispositivi endovascolari per il per procedure minimamente invasive, come stent e filtri embolici. Nello specifico, gli stent costituiti in SMA, possiedono la capacità di autoespandersi a livello dell'arteria danneggiata, una volta rimosso il catetere di protezione. Questa particolare caratteristica, ha fatto lievitare negli anni il mercato degli stent, portando ad una vasta gamma di scelta tra diversi design e processi produttivi. Questo sviluppo improvviso ha aperto diversi filoni di R&D allo scopo di migliorare le prestazioni dei dispositivi, ma ha reso complicata la standardizzazione delle procedure. Le analisi agli elementi finiti (FEA) si sono dimostrate uno strumento molto affidabile per la valutazione dei dispositivi e delle loro caratteristiche, ed uno dei componenti fondamentali di una FEA è la corretta modellazione delle proprietà del materiale dello stent. Per questo motivo, la creazione di un modello costitutivo affidabile e robusto dal punto di vista computazionale è una delle operazioni chiave per ottenere una FEA ottimale. Lo scopo di questa tesi

é quello di fornire ad un utente medio/esperto di risolutori agli elementi finiti (ad esempio Abaqus) tutti gli strumenti di base per la comprensione e l'implementazione di un modello costitutivo per SMA. A partire dalla descrizione di un modello SMA accurato e robusto [16], le equazioni cardine del modello costitutivo verranno dettagliati e circostanziati. Nel capitolo successivo, l'implementazione del modello costitutivo in ambiente Abaqus, verrà descritta dando particolare attenzione alle differenze, in termini di requisiti e di struttura del codice, tra l'implementazione del modello in un risolutore implicito. In quest'ottica una subroutine codificata in implicito, ma con una struttura fruibile per un risolutore esplicito, é stata codificata in codice Fortran e testata con dei semplici test uniassiali. In seguito, i risultati dei test sono stati confrontati con quelli ottenuti da altri modelli. Nello specifico, la subroutine sviluppata é stata, in prima battuta, confrontata con un codice identico ma con una struttura valida per un risolutore implicito. Una volta fatto ciò la subroutine é stata confrontata con una subroutine implicita, ricavata da un modello diverso dall'originale [22] e i risultati sono stati confrontati. I risultati di questi test mostrano, come ci si aspettava, una perfetta correlazione tra i dati della simulazione implicita e quelli della simulazione esplicita. Per quanto riguarda il secondo confronto, la corrispondenza ,a seguito di una fase di calibrazione dei parametri del modello, risulta essere eccellente. Nell'ultima parte di questa tesi, la subroutine sviluppata é stata introdotta in due FEA decisamente più complesse in modo da valutare, in modo qualitativo, le capacità del codice nell'ambito di analisi più complesse.

Contents

| | | |
|----------|--|-----------|
| 1 | Background and aims | 5 |
| 1.1 | Smart materials: introduction to shape memory alloys | 5 |
| 1.1.1 | A little bit of history | 7 |
| 1.2 | SMA properties | 8 |
| 1.2.1 | Pseudoelasticity and SME effects. | 9 |
| 1.2.2 | Kink resistance | 12 |
| 1.2.3 | Biocompatibility | 12 |
| 1.2.4 | Constant unloading stresses; | 13 |
| 1.2.5 | Hysteresis | 13 |
| 1.2.6 | Fatigue resistance | 13 |
| 1.3 | SMA application field | 14 |
| 1.4 | SMA behavior and modelization issues | 16 |
| 1.5 | Thesis aim and organization | 18 |
| 2 | SMA constitutive model theoretical description | 20 |
| 2.1 | Shape memory alloy macroscopical properties and modelization | 21 |
| 2.2 | Review of Shape Memory alloys models. | 24 |
| 2.3 | Souza 3D phenomenological model | 27 |
| 2.3.1 | Time-continuous model | 27 |
| 2.3.2 | Auricchio and Petrini improvements | 30 |
| 2.3.3 | Time-discrete model and solution algorithm | 32 |

| | |
|---|-----------|
| <i>CONTENTS</i> | 5 |
| 2.3.4 Model parameters | 34 |
| 2.3.5 Considerations about Souza model | 36 |
| 2.3.6 Stress-strain examples | 37 |
| 2.4 Lagoudas phenomenological model | 37 |
| 2.4.1 Considerations about Lagoudas model | 41 |
| 3 Shape memory alloy VUMAT subroutine implementation | 43 |
| 3.1 Finite Element Method: a quick overview | 44 |
| 3.2 User material subroutines: UMAT versus VUMAT | 46 |
| 3.2.1 UMAT subroutine | 47 |
| 3.2.2 VUMAT subroutine | 48 |
| 3.2.3 Comparison between VUMAT and UMAT | 50 |
| 3.3 SMA VUMAT implementation. | 50 |
| 3.4 SMA VUMAT tests | 53 |
| 3.4.1 Pseudoelasticity test | 54 |
| 3.4.2 Shape Memory Effect test | 56 |
| 3.5 Results and comparison | 57 |
| 3.5.1 Results discussion | 57 |
| 3.5.2 Comparison with the UMAT code | 59 |
| 3.5.3 Comparison with the SMA_UM | 61 |
| 4 Realistic examples | 65 |
| 4.1 Pseudo-elastic stent compression example | 66 |
| 4.2 Microgripper example | 70 |

Chapter 1

Background and aims

This chapter is focused on the description of shape memory alloys (SMA) behavior. Starting from the role of innovative materials in the technological progress, SMA discovery and evolution will be described. In order to briefly explain the reasons of the great success of SMA, their physical properties will be detailed with particular care to pseudoelasticity and shape memory effect. After that, following a quick overview of SMA application fields, the main issues related to the modeling of SMA mechanical behaviour will be discussed. At the end of the chapter, the aim and the structure of this thesis will be described.

1.1 Smart materials: introduction to shape memory alloys

The last 40 years represent an important turning point from a technological point of view. Indeed this period of time coincides with the transition between the "Synthetic materials age" to "Smart materials age" (Gandhi and Thompson, 1992, [1]).

Material discoveries are the engine of technology evolution and, in particular, of practical consequences in way of life (Figure 1.1). The main feature

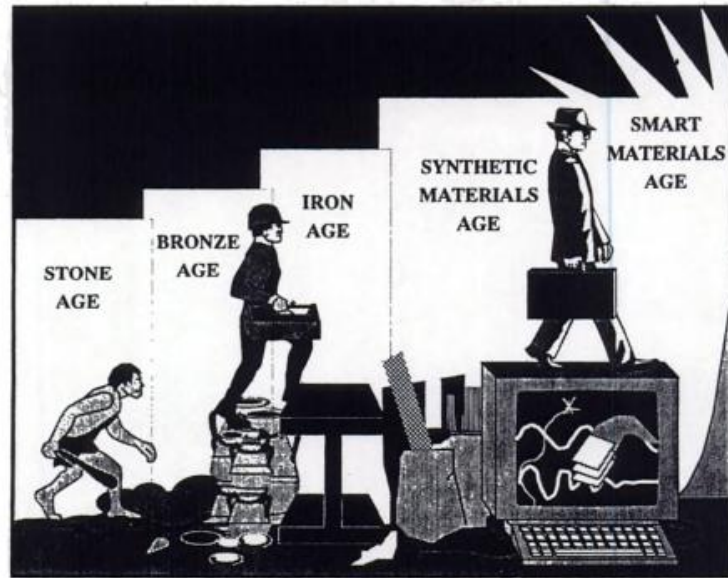


Figure 1.1: The eras of material science (Gandhi and Thompson, 1992).

of smart materials is the capability to respond, after an environmental stimulus, with particular changes in some variables e.g., temperature, moisture, electric or magnetic fields, pH, and stress. Depending on changes in some external conditions, smart materials can change their physical properties and/or their structure. There are a number of types of smart material, some of which are common in the ordinary life (see [2] for details). For example piezoelectric materials, defined as materials that produce a voltage when stress is applied (the effect exists also in the reverse direction), are commonly used for a huge variety of applications, from components for loudspeakers to fuzes for rocket-propelled grenades. As their variety, application field for smart materials is huge, and varies e.g., from electronic engineering to civil engineering, passing through aeronautical and medical applications.

1.1.1 A little bit of history

In this context of rapid evolution, shape memory alloys (SMA) entered on tiptoe. In fact the discovery of shape memory in AuCd and CuZn occurred with little fanfare in somewhat obscure technical papers with little, if any, follow-on work [3]. The real progress for SMA introduction in engineering applications occurred with the discovery of NiTiNOL (nickel titanium alloy, NOL was in honor of the discovery at the Naval Ordnance Laboratory) by Buehler and coworkers in 1962 while investigating materials useful for heat shielding [4]. It was noticed that in addition to its good mechanical properties, comparable to some common engineering metals, the material also possessed a shape recovery capability. After the NiTiNOL discovery, there was suddenly a great deal of commercial interest, and many commercial applications have been developed, especially in automotive and aeronautical fields.

Nevertheless several problems, like non-linear tensile properties, hysteresis, fatigue, and adiabatic heating and cooling effects, coupled with high costs for the production, convinced many companies that shape memory was not financially advantageous. Despite this discouraging frame, the continuous effort in material research revealed the potentials for those alloys. Moreover, the development of different models for material performance prediction, permitted to understand clearly the thermomechanical processing route and the environmental parameters. Thank to 20 years of studies in their behavior, SMA are, nowadays, an "household" word in the engineering world. A higher quality and reliability, in combination with a significant decrease in prices, thanks to a larger market share, allows moreover to consider new potential applications with tight budgets or cost factors.

1.2 SMA properties

The main features of SMA are:

- *Pseudoelasticity* (PE): capability to recover strains after stress-induced large deformations;
- *Shape memory effect* (SME): capability to recover plastic strains after an heating process;

These peculiar properties are joined with the following properties:

- Kink resistance;
- Biocompatibility;
- Constant unloading stresses;
- Hysteresis;
- Fatigue resistance;

These properties explain the large diffusion, in the last 20 years, of SMA in the production of a wide variety devices, in particular for mini-invasive techniques in medical applications. In this section, all the listed properties will be described in detail, with particular regard to PE and SME.

1.2.1 Pseudoelasticity and SME effects.

Both PE and SME effects are strongly related to the martensitic transformation and the basic notion of this phenomenon is first given. The martensitic transformation (MT) is a diffusionless phase transformation in solids, in which atoms move cooperatively, often by a shear-like mechanism. The transformation from one structure to the other one does not occur by diffusion of atoms, but rather by shear lattice distortion.

This particular phenomenon is associated with the crystallographic organization of SMA, characterized by a two-solid phases structure:

- Austenitic phase (parent phase): characterized by an high symmetric crystallographic structure. This phase is stable at high temperatures ($T > A_f$ austenite finish transformation temperature);
- Martensitic phase: stable at temperatures $T < M_f$ with M_f martensite finish transformation temperature, presents a low symmetry structure (tetragonal, orthorhombic or monoclinic);

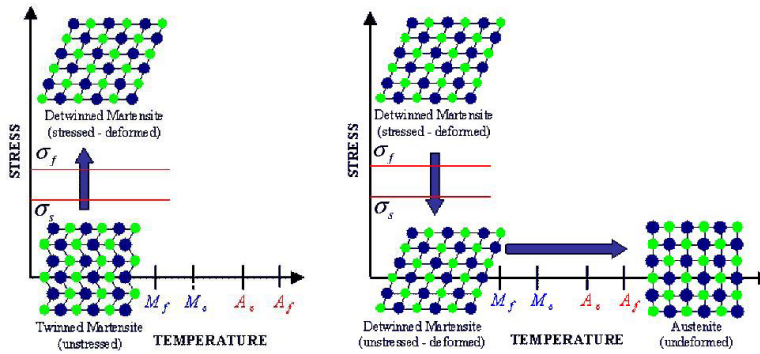


Figure 1.2: (*left*) Schematic of the shape memory effect of an SMA showing the detwinning of the material with an applied stress [14]. (*right*) Schematic of the shape memory effect of an SMA showing the unloading and subsequent heating to austenite under no load condition [14]

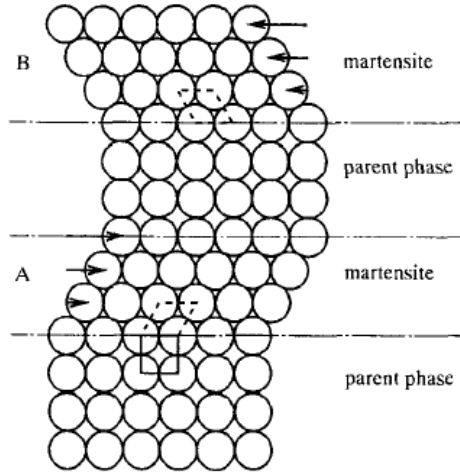


Figure 1.3: A schematic model of martensitic transformation [13]

The martensite in region A has the same structure of martensite in region B, but exhibits different orientation. This assumption suggests that martensite can exist in two different configurations: stress-free martensite, characterized by a twinned multi-variant crystallographic structure, not related to any macroscopic deformation, and stress-induced martensite, characterized by a typical detwinned configuration with a single variant crystallographic structure, which aligns variants along a predominant direction, hence associated with macroscopic deformation [19]. It is important to remark that the martensitic transformation in SMA consists mainly in a shear, without volume change [13],[14].

The transition between different phases is the key to fully describe the behavior of SMAs, and is clear that all the phenomenons are ruled by the strong connection between mechanical effects (loadings) and thermal effects (change in temperature).

A load (at a temperature greater than A_f) causes, initially, an elastic deformation in austenite phase (①), then, if the deviatoric part of the stress reaches the value of σ^{AS} the transition between austenite to single-variant martensite ($A \rightarrow SM$) begins (②). This phase exhibits a wide plateau due to the nature of the transformation phase. Once the austenite has been converted, an elastic deformation for martensite phase can be seen (③). When the load is removed, the martensitic phase, after an elastic recover phase (④), tends to the reverse transformation (⑤), in reason of the instability of martensite phase at high temperatures. This phenomenon causes the complete recovery of the strain (pseudo elastic effect). In this way, Nitinol is able to recover large deformations (in the order of 10%).

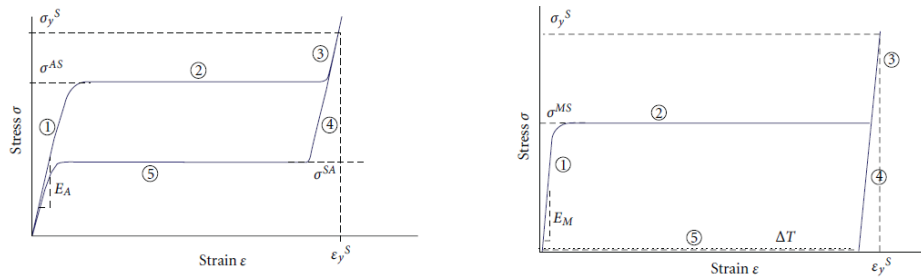


Figure 1.4: (*left*) Schematic of a pseudo-elastic stress-strain diagram, (*right*) Stress-strain-temperature data exhibiting the shape memory effect for a typical NiTi SMA [8].

In the other way, at a temperature lower than M_F , multi variant martensite phase is present. A load such that the deviatoric part of the stress is greater than σ^{MS} , induces, after an elastic deformation step (①), the multi variant to single variant martensite transformation (②), and a single variant elastic deformation step (③). After the load removal, a residual strain takes place (④). If the material is heated at a temperature around A_f , the residual strain is fully recovered at zero stress (⑤), in reason of the transition between

single variant martensite and austenite phase (shape memory effect).

1.2.2 Kink resistance

Kink resistance or, more appropriately, crush recoverability, is an important feature of NiTiNOL, even more than PE and SME in some applications. When strains are locally increased beyond the plateau strain, stresses increase markedly. This causes strain to partition to the areas of lower strain, instead of increasing the peak strain itself. This phenomenon can be very dangerous for device performances, and it is not uncommon in steel devices. In NiTiNOL devices, kinking, or strain localization, is prevented by creating a more uniform strain than could be realized with a conventional material. This property is widely used in medical applications, especially in laparoscopic surgery, where the ability to lead the device through side branches or around sharp bends is vital.

1.2.3 Biocompatibility

This feature is obviously related to medical application and can be roughly defined as the ability of a material to be not rejected by the human body. Biocompatibility is directly related to the corrosion behavior of the material in a specified solution and the tendency for the alloy to release potential toxic ions. Experimental studies, generally indicate that nitinol has extremely good biocompatibility. This is due to the tendency of Nitinol surfaces to be covered with TiO_2 oxides with only a minor amount of nickel under normal conditions [6]. The TiO_2 layer has a double purpose:

- Increase in the stability of the surface layers by protecting the bulk material from corrosion;
- Creation of a chemical barrier against Nickel oxidation, potentially toxic for the organism.

1.2.4 Constant unloading stresses;

This feature is directly connected with SE and martensitic transformation. Infact stresses observed in a NiTiNOL device are, for a wide range of strains, temperature-driven and not strain-driven as in conventional materials. This effect is due to the wide plateau that coincides to the AB martensitic transformation. So, if temperature remains substantially constant, is possible to design devices that applies a constant stress over a wide range of shapes.

1.2.5 Hysteresis

The superelastic hysteresis, as described in the chapter introduction, has been considered a drawback because it reduces the energy storage efficiency: a device requiring 5 J for deformation, may only return 2 J of mechanical energy upon unloading [5]. This hysteresis is a desirable feature in stent design, for example. A superelastic stent should provide only a very light chronic outward force against a vessel wall, and at the same time be highly resistant to crushing compliant in one direction, and stiff in the other.

1.2.6 Fatigue resistance

It is well known that nitinol offers exceptional fatigue resistance in high strain, strain-controlled environments, while it may well fatigue rapidly in stress-controlled environments- Practically speaking, most fatigue environments in the body involve irregular cyclic motion against highly compliant tissue, and thus are a combination of stress and strain-control. Fatigue is also complicated by the superposition of a mean stress or strain on top of the cyclic component. As example of NiTiNOL fatigue study, Pelton et al. [7] tested the combined effects of cardiac pulsatile fatigue and vessel oversizing in vascular stents application. In particular, displacement controlled fatigue tests were performed and fatigue data were collected with combinations of simulated oversizing conditions and pulsatile cyclesm with both experimental

and computational tools .

1.3 SMA application field

As described previously, SMA applications cover a huge variety of fields. Many alloy systems show shape memory behavior but only a few of them have been developed for a large scale market. Nowadays almost all the new SMA-applications are based on NiTi or ternary NiTi-Cu and NiTi-Nb alloys (in a percentage around 90% [9]). NiTi SMA predominance is due to the improved strength and ductility respect to other alloy. NiTi SMAs are available in the shape of thin wires and thin films, and have a higher electrical resistivity making electrical activation simpler. Concerning to medical applications, NiTi SMA show high biocompatibility, and high resistance to corrosion. For these reasons, NiTi SMA replaced Cu-based SMA although the industrial processes for the production result more difficult and expensive. Looking at the literature review on SMA applications topic, is clearly visible the partition between medical and non medical applications (e.g.,[3] and [9]). Medical applications includes (for the details see [8], [10], [5]):

- Cardiovascular applications: Starting from self-expandable stents, passing through embolic filters and stent grafts, NiTiNOL is widely used in minimally-invasive surgery;
- Orthopaedics applications: The application of nitinol in orthopaedics is a promising market but not fully realized yet. Although much research has gone in the direction of correction rods, compression staples and fracture fixators;
- Clinical instruments: There is a growing market for nitinol in clinical instruments, especially for biopsy forceps, NiTiNOL guidewires, tissue ablaters and retrieval baskets for laparoscopy;

- Ortodontic applications: SMA are widely used for Wires, palatal arches, distractors and endodontic files. Ortodontic applications werethe first SMA medical applications available on the market;
- Other applications: birth control devices, laparoscopic inguinal hernio-plasty, stapes prosthesis, colonic anastomosis are some of SMA devices developed in the last years;

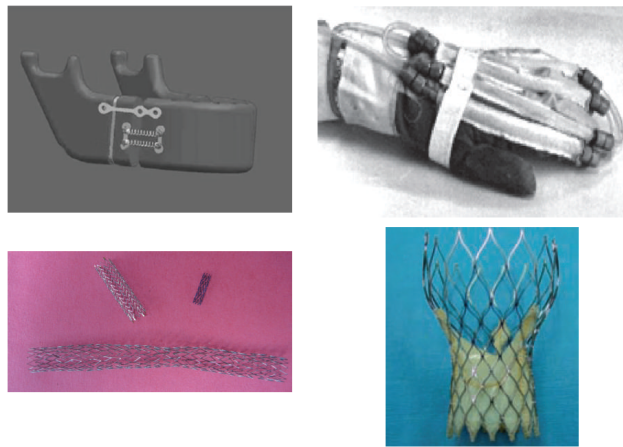


Figure 1.5: Short overview of SMA's medical applications: (*top left*) Orthodontic distractors [11], (*top right*) Gloves with SMA wires [12], (*bottom left*) SMA stents [8], (*bottom right*) CoreValve aortic valve <http://www.medtronic.com/corevalve/ous/index.html>.

Concerning to non medical applications Van Humbeeck [9] described:

- Fashion, decoration and gadgets: This application field produce devices for ordinary life like eye glass frames (bow bridges and temples), frames for brassieres and antennas for portable cellular telephones;
- Couplings and fasteners: SMA are widely used for heat-recoverable couplings, heat-to-shrink fasteners and dematable connectors since the

70's. In fact, a coupling to connect titanium hydraulic tubing F-14 aircraft was the first large scale application of SMA in 1971;

- Microactuators: SMA properties can be exploited to realize thermal actuators. Following the division given by Otsuka et al.[13] is possible to divide SMA actuators in applications where the device is both sensor and actuator, and applications where the device only performs a complete controlled action. The first class includes ,e.g.,many safety control devices e.g. water kettles with shape memory actuated heat cut off, coffee makers, thermal protection device. The second class includes, e.g., devices for the control of the environmental temperatures and flow control devices for air conditioners;
- Other applications: Adaptive materials, hybrid composites and devices that use the high damping capacity of SMA;

1.4 SMA behavior and modelization issues

As described in the properties section, SMA are characterized by a variety of peculiar features, that make these materials very attractive for industrial market, but , at the same time, makes difficult to fully understand their behavior and to predict their performances. As suggested by Arghavani [15], is possible to partition the SMA behaviors into two families:

- Primary effects: include pseudo-elasticity, shape memory effect as well as variant reorientation;
- Secondary effects: cover other effects which may turn out to be relevant in some practical cases.

The secondary effects include tension-compression asymmetry, different elastic moduli for austenite and martensite phase, progressive strain under

cyclic loadings and thermal-mechanical coupling (as illustrated in fig. 1.6). As described in section 1.1.1 contemporarily to experimental investigations, in the last 20 years a big effort has been also devoted to define constitutive models able to describe the main SMA behaviours. The main challenge for model theoretical conception and computational implementation, is to predict primary effects described previously, with regard also for secondary effects in relation with the practical implementation of the model.

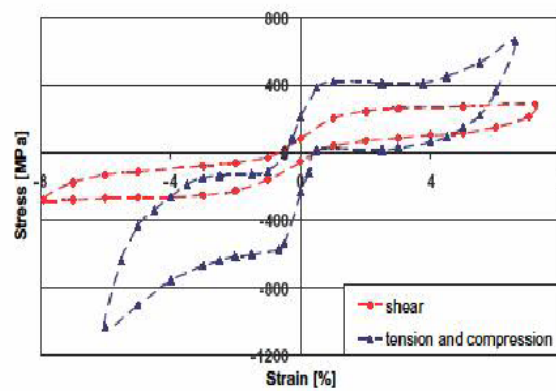


Figure 1.6: Asymmetric behavior under tension, compression and torsion (Orgeas and Favier , 2008)

1.5 Thesis aim and organization

As highlighted by the brief introduction, SMA, in reason of their peculiar mechanical properties, offer many interesting possibilities in the development of smart devices, especially for medical applications. Despite of the great commercial interest in this topic, there's still the strong need of investigation tools, focused on the optimization of devices design. These tools, based on engineering methods, have to predict the behavior of the devices taking into account the material properties. Finite elements analysis (FEA), result a valid tool to evaluate the design of devices and to predict the material performance. In particular, Abaqus, one of the most used FEA commercial solver, implements material constitutive equations in the form of user subroutine, coded in Fortran language, with different organization for implicit (UMAT subroutine) and explicit (VUMAT subroutine) FEA. The aim of this thesis is to analyse an attractive SMA model [16] and to elaborate a user subroutine, coded in order to cross between UMAT and VUMAT with few modifications. This subroutine has been tested and compared with other two available subroutines. In the final part, the subroutine has been implemented in two realistic simulations, studied to highlight the principal SMA features. The thesis is structured as follows:

- **Chapter 2:** After a quick overview on the SMA behavior models available, Souza modified model [16], [19], is described, with focus on theoretical modelization and basic equations;
- **Chapter 3:** Souza model numerical framework and user subroutine implementation issues will be deeply described. In particular, code modification to convert implicit to explicit subroutine will be analysed. Then, the subroutine will be tested on a simple Finite Element model and compared with two others subroutines.
- **Chapter 4:** SMA subroutine is exploited for two realistic simulations.

The first one, structured to emphasize PE, consists in a carotid stent portion compression test, while the second one simulates the behavior of a micro-gripper based on SME.

Chapter 2

SMA constitutive model theoretical description

The fundamentals of SMA behavior and their application field have been introduced in the first chapter. This chapter introduces the basics about the modeling of SMA thermomechanical behavior. The first section describes the basics for the modeling of SMA macroscopical properties, with primary and secondary effects, and the needs for a FEA implementation. After a brief review of SMA models classification and state-of-art, Souza model [16] will be described, highlighting also the improvements introduced by Auricchio and Petrini [19]. In particular, basic equations and theoretical framework of the continuous model will be detailed, with care in describing PE and SME. Following the theoretical point of view, the discretization of the model will be described, in order to convert it in a format suitable for FEA. Finally, Lagoudas model [22] will be briefly described, in reason to compare the different implementations, which will be discussed in chapter 3.

2.1 Shape memory alloy macroscopical properties and modelization

As discussed in the previous chapter, SMA are metallic alloys that have the ability to recover from significant deformation, thereby regaining a previous shape, when subjected to specific thermomechanical loads (primary effects), mixed with a variety of other peculiar phenomenons, called secondary effects. A satisfactory description of all these features is not trivial, and the task become even harder when the material behavior has to be “encaged” into a discrete framework for FEA. In particular, in order to improve computational testing of new devices, the constitutive model should be able, starting from experimental data (fig.2.1), to describe the macroscopic effects that could be important for the specific application. In fact developing a 3D SMA model able to consider many SMA complicated behaviors does not mean that it is an effective SMA model in engineering applications. To this end, besides research activities in SMA modeling, it is necessary to decide which behaviors should be included in modeling according to engineering and computational requirements [15].

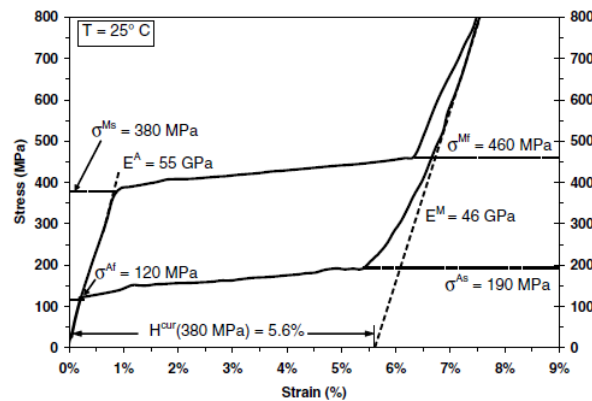


Figure 2.1: Pseudoelastic loading/unloading results and derivation of parameters for various testing temperatures of 25 Celsius degrees. [14]

There are many approaches to define the constitutive relations for SMA, but this section will focus on the procedure for obtaining constitutive equations using internal state variables. Starting from the basics of Continuum Mechanics, the fundamental components are:

- Kinematics: is the study of body configuration changes. Kinematics describes the geometry of motion and deformation of a body, without considering the cause of that motion and deformation.
- Equilibrium: is the study of the body equilibrium conditions. Equilibrium includes the relations for the measurement of the internal forces. This component can be described in terms of conservation laws (mass, linear momentum, angular momentum and energy).
- Constitutive relations: this component takes in account the phenomenological nature of the body. Constitutive equations are in general expressed as relations between internal forces and measures of the body configuration, like a bridge between equilibrium and kinematics.

These equations represent the fundamentals of mechanics of solids, and constitutive relations allow to have a system with unique solutions (see Gurtin [29]). Constitutive equations are mathematical models able to describe the principal features of a material behavior. SMA are materials that undergo a phase transformation and therefore are characterized by a sequence of thermodynamic states that can be described by the introduction of other variables, called internal state variables. The thermodynamic state of a SMA material can be fully determined by a combination of external and internal state variables. Starting from the previous assumption is reasonable, as described by Lagoudas [14], pass through a basic entity, called thermodynamic potential, to derive the constitutive equations for SMA behavior. A thermodynamical potential, is a function that characterizes a certain thermodynamic state of a material and it depends on state variables,

both external and internal. Four thermodynamic potentials are commonly defined, according to a certain choice of the independent state variables. These four thermodynamic potentials are the specific internal energy, u , the specific Helmholtz free energy, Ψ , the specific enthalpy, h , and the specific Gibbs free energy, G , as specific quantities defined per unit of mass. The internal energy, u , can be defined as a measure of kinetic and potential energy of the material points within the material system. The Helmholtz free energy, Ψ , is defined to be the portion of the internal energy available for doing work at constant temperature, whereas enthalpy is the portion of internal energy that can be released as heat at constant applied stress. The Gibbs free energy, G , is finally the portion of enthalpy available for doing work at constant temperature. In theory, all the thermodynamic potentials are suitable to be the basic for the constitutive relations derivation, but only Gibbs and Helmholtz free energies are commonly used, in the reason of the difficulty to measure entropy and internal energy. The choice between Gibbs and Helmholtz free energies is based on the state variable the model projectist can control during experimental measurement, i.e., stress or strain. To put it briefly the main steps to derive constitutive relations for SMA are:

- Choice of internal state variables: the microstructural changes due to phase transformation should be represented by a set of internal variables. Different choices can change deeply the model complexity, and the related features.
- Kinematics and thermomechanical assumptions: in this step, starting from experimental observation, it is possible to set some conditions to simplify the system, such as small strain regime or additive decompositions for state variables. Moreover, it is possible to choose the appropriate thermodynamic potential for the constitutive relations derivation.

- Evolution of Internal State Variables: In this step, the evolution laws for the internal variables are defined following the approach described by Simo and Hughes [20]. To define a rate-independent plasticity model, the evolutionary behavior of plastic strain must be defined with a relation called *flow rule*.

2.2 Review of Shape Memory alloys models.

Many models are available to describe the SMA behavior. As described in the previous section, the main requirement for a model has to be the prediction of the primary phenomenon related to SMA (PE and SME), but also secondary effects could be important, i.e. asymmetric response in tension and compression, detwinning of martensite, two-way shape memory effect and reorientation effects. It is possible to index the wide variety of models focusing on different aspects i.e. chronology, microspical or macroscopical approaches, differences in control and state variables with related thermo-mechanical potentials. In this section, following the classification suggested by Arghavani [15], SMA models can be classified into two big families:

- Models without internal variables
- Models with internal variables

Models without internal variables describe SMA behaviors without including quantities representing austenitic and martensitic mixture, using only strain, stress, temperature and entropy. Polynomial models and hysteresis models can be included in this family. The first describes the material behavior starting from a polynomial free energy function, which can be derived to get the constitutive equations, while the latter creates the constitutive relations starting from mathematical properties, often neglecting the physical aspects underlying the material behavior. The introduction of

internal variables to describe the material internal structure, in combination with the control variables (stress or strain, and thermal variables such as temperature and entropy) allow to describe the material constitutive relations, accounting for the physical meaning underlying the experimental data. The internal variables typically include one or more phase fractions and/or macroscopic transformation strains. In these section some of the works related to this thesis will be introduced, for a more detailed overview see [14], [15]. The first model based on internal variables was proposed in 1982 by Tanaka and Nagaki [21], it was characterized by an exponential hardening rule and by the material properties remained constant during transformation phase. This model was theoretically studied for 3D problems, but its implementation was restricted to 1-D problems, until Boyd and Lagoudas [22] extended the formulation, in order to permit the 3D implementation. Other models are Bondaryev and Wayman model [23], based on classical plasticity theory and Liang and Rogers model [24], characterized by cosine kinetics for the internal variable martensite volume fraction. In 90's, the growing number of SMA applications, in particular on biomedical applications, enhanced the creation of 3D phenomenological models (oriented to the computational testing of devices). 1-D implementation remained active for the description of SMA's secondary effects, i.e., martensit volume fraction decomposition [25], in reason of its simplicity, and for the wide use of SMA wires in many applications . In this context, remarkable works are Raniecki and Lexcellent [26]) and Leclercq and Lexcellent [27] models, able to describe the macroscopic thermo-mechanical behavior using two internal variables, in order to allow modeling of both detwinned and twinned martensite. In 1996 Lubliner and Auricchio considered a 3D response using a Drucker-Prager-type surface to describe the critical stresses for pseudoelastic transformation with exponential hardening law. Moreover, this study was oriented to finite element implementation (this work is based on the generalized plasticity the-

ory [17]). Souza et al. ([16]) proposed in 1998 a model able to describe the main features of polycrystalline shape memory materials for 3D implementation. Auricchio and Petrini improved this model, in order to increase its robustness for finite element implementation [19]. Qidwai and Lagoudas ([28]) proposed a comprehensive modeling with tension-compression asymmetry, starting from the previous work of Boyd and Lagoudas [22]. In this model several different transformation surfaces were tested. In this wide variety of models, with different approaches and features that can be implemented, the constitutive law proposed by Souza et al. [16] have been chosen for this dissertations for its attractive features.

2.3 Souza 3D phenomenological model

Souza model, developed within the framework of phenomenological continuum thermodynamics [17], is able to describe PE and SME with a simple and robust solution algorithm based on return-map procedure [20]. This feature leads to a robust model suitable for FEA, and the simulation complex SMA devices.

2.3.1 Time-continuous model

The authors chose strain, ε , and the absolute temperature, T , as control variables and the second-order transformation strain tensor, \mathbf{e}^{tr} , as internal variable. The model has been developed under small strain regime, justified by the fact that the approximation of large deformations and small strains is valid for several application. The quantity e^{tr} has the role of describing the strain associated to the phase transformations. This variable is assumed traceless, in reason of experimental results indicating no volume changes during the phase transformation [18]. Furthermore the value of transformation strain norm (euclidean norm) is assumed always less than the value of ε_L , defined as the transformation strain norm value at the end of the transformation phase (ε_L , defined as a material parameter).

$$\|\mathbf{e}^{tr}\| \leq \varepsilon_L, \quad (2.1)$$

ε_L can be derived with a simple uniaxial test and it represents the value of transformation strain at the end of transformation phase. The following additive decomposition have been used for ε :

$$\varepsilon = \frac{\theta}{3} \mathbf{1} + \mathbf{e}, \quad (2.2)$$

where $\theta = \text{tr}(\varepsilon)$ and e are, respectively, the volumetric and the deviatoric

part of the total strain ε , while $\mathbf{1}$ is the second-order identity tensor.

The free energy density function, or Helmholtz free energy Ψ , is defined to be the portion of the internal energy available for doing work at constant temperature, and represents the root for the development of many constitutive relations.

For a polycrystalline SMA material Ψ is expressed as

$$\begin{aligned} \Psi(\theta, \mathbf{e}, T, \mathbf{e}^{tr}) = & \frac{1}{2}K\theta^2 + G\|\mathbf{e} - \mathbf{e}^{tr}\|^2 - 3\alpha K\theta(T - T_0) + \beta\langle T - T^* \rangle \|\mathbf{e}^{tr}\| + \\ & \frac{1}{2}h\|\mathbf{e}^{tr}\|^2 + (u_0 - T\eta_0) + c \left[T - T_0 - T \log \left(\frac{T}{T_0} \right) \right] + \mathcal{I}_{\varepsilon_L}(\mathbf{e}^{tr}), \end{aligned} \quad (2.3)$$

where K and G are, respectively, the bulk and the shear modulus, α is the thermal expansion coefficient, β is a material parameter associated with the stress-temperature relation, T_0 is the temperature below which only martensite phase is stable, h is the hardening parameter associated with the transformation phase, c is the heat capacity, and u_0 , η_0 and T_0 are, respectively, the internal energy, the entropy and the temperature at the reference state, while the symbol $\langle a \rangle$ is the positive part function. The component $\mathcal{I}_{\varepsilon_L}(\mathbf{e}^{tr})$ is set equal to an indicator function introduced to satisfy the previous constraint on the transformation strain norm:

$$\mathcal{I}_{\varepsilon_L}(\mathbf{e}^{tr}) = \begin{cases} 0 & \text{if } \|\mathbf{e}^{tr}\| \leq \varepsilon_L \\ +\infty & \text{otherwise} \end{cases} \quad (2.4)$$

Deriving the Ψ function with different arguments is possible to highlight the different stress components

$$\left\{ \begin{array}{l}
 p = \frac{\partial \Psi}{\partial \theta} = K [\theta - 3\alpha(T - T_0)], \\
 \mathbf{s} = \frac{\partial \Psi}{\partial \mathbf{e}} = 2G(\mathbf{e} - \mathbf{e}^{tr}), \\
 \eta = -\frac{\partial \Psi}{\partial T} = \eta_0 + 3\alpha K \theta - \beta \|\mathbf{e}^{tr}\| \frac{\langle T - T^* \rangle}{|T - T^*|} + c \log \left(\frac{T}{T_0} \right), \\
 \mathbf{X} = -\frac{\partial \Psi}{\partial \mathbf{e}^{tr}} = \mathbf{s} - \beta \langle T - T^* \rangle \frac{\mathbf{e}^{tr}}{\|\mathbf{e}^{tr}\|} - h \mathbf{e}^{tr} - \gamma \frac{\mathbf{e}^{tr}}{\|\mathbf{e}^{tr}\|},
 \end{array} \right. \quad (2.5)$$

\mathbf{s} and p represent, respectively, the deviatoric and the volumetric part of the stress. \mathbf{X} represents a stress-like quantity related to transformation strain and can be considered as the driving force for phase transformations processes. It is important to note that if $\mathbf{e}^{tr} = 0$ the transformation stress \mathbf{X} remains undetermined. To solve this problem the authors proposed this different definition for \mathbf{X} , in the step of nucleation of the product phase

$$\mathbf{X} = R \frac{\mathbf{S}}{\|\mathbf{S}\|} \quad (2.6)$$

This relation can be proved with the assumption of an hypothetical process starting with $\mathbf{e}^{tr} = 0$ and $\dot{\mathbf{e}}^{tr} \neq 0$. Assuming that $\|\mathbf{S} - \mathbf{X}\| = \beta \langle T - T^* \rangle + h \|\mathbf{e}^{tr}\|$ holds for \mathbf{e}^{tr} in a neighbourhood of 0, it follows by continuity that $\|\mathbf{S} - \mathbf{X}\| = \beta \langle T - T^* \rangle$. Therefore, if phase transformation is expected there will be

$$\|\mathbf{S}\| = \|\mathbf{S} - \mathbf{X} + \mathbf{X}\| \leq \|\mathbf{S} - \mathbf{X}\| + \|\mathbf{X}\| = \beta \langle T - T^* \rangle + R \quad (2.7)$$

this relation is obtained taking in account the transformation, leads to $\|\mathbf{X}\| = R$.

Strict inequality in eq. 2.7 is not consistent, because the flow rule imposes that $\dot{\mathbf{e}}^{tr}$ must have the same direction of $\|\mathbf{X}\|$, and \mathbf{e}^{tr} as well, when integrated in a short process. This is impossible because \mathbf{e}^{tr} should point toward $\|\mathbf{S} - \mathbf{X}\|$, as described in \mathbf{X} definition (eq.2.5)

Moving back to the model description, the derivation of $\mathcal{I}_{\varepsilon_L}(\mathbf{e}^{tr})$ creates the variable γ defined such that

$$\begin{cases} \gamma = 0 & \text{if } \|\mathbf{e}^{tr}\| < \varepsilon_L, \\ \gamma \geq 0 & \text{if } \|\mathbf{e}^{tr}\| = \varepsilon_L, \\ \partial\mathcal{I}_{\varepsilon_L}(\mathbf{e}^{tr}) = \gamma\mathbf{e}^{tr}/\|\mathbf{e}^{tr}\| \end{cases} \quad (2.8)$$

while the yielding is ruled by the following limit function

$$F(\mathbf{X}) = \|\mathbf{X}\| - R, \quad (2.9)$$

where R is a positive material parameter that can be defined as the radius of the elastic domain. Finally, the flow rule for the internal variable and the classical Kuhn-Tucker conditions take the form

$$\dot{\mathbf{e}}^{tr} = \dot{\zeta} \frac{\partial F}{\partial \mathbf{X}} = \dot{\zeta} \frac{\mathbf{X}}{\|\mathbf{X}\|}, \quad (2.10)$$

$$\begin{cases} \dot{\zeta} \geq 0, \\ F \leq 0, \\ \dot{\zeta} F = 0. \end{cases} \quad (2.11)$$

where $\dot{\zeta}$ plays a role similar to the plastic consistent parameter.

2.3.2 Auricchio and Petrini improvements

Auricchio and Petrini [19] analysed the Souza model described in the previous section and introduced some modifications, in order to improve the model robustness for FEA. In the previous section the transformation stress \mathbf{X} dependance on the derivative of the transformation strain has been highlighted as a critical point when \mathbf{e}^{tr} is close to 0, making the derivative and \mathbf{X} , undefined. To overcome this problem, the authors proposed to replace the Euclidean norm $\|\mathbf{e}^{tr}\|$ with the regularized norm $\overline{\|\mathbf{e}^{tr}\|}$, defined as:

$$\overline{\|\mathbf{e}^{tr}\|} = \|\mathbf{e}^{tr}\| - \frac{\delta^{\delta+1/\delta}}{\delta-1} (\|\mathbf{e}^{tr}\| + \delta)^{\delta-1/\delta} \quad (2.12)$$

where δ is a user-defined parameter which controls the smoothness of the regularized norm. In this way the quantity $\overline{\|\mathbf{e}^{tr}\|}$ is always differentiable, even for $\|\mathbf{e}^{tr}\| = \mathbf{0}$. Moreover the authors introduced another form for the yielding function $F(\mathbf{X})$, as function of second (J_2) and third (J_3) invariants of the transformation stress tensor \mathbf{X}

$$F(\mathbf{X}) = \sqrt{2J_2} + m \frac{J_3}{J_2} - R \quad (2.13)$$

$$J_2 = \frac{1}{2}((\mathbf{X}^2 : \mathbf{1})) \quad (2.14)$$

$$J_3 = \frac{1}{3}((\mathbf{X}^3 : \mathbf{1})) \quad (2.15)$$

where m is a material parameter. Both R and m can be associated to the uniaxial critical stress in tension σ_t and in compression σ_c by the relations

$$R = 2\sqrt{\frac{2}{3} \frac{\sigma_t \sigma_c}{\sigma_c + \sigma_t}} \quad (2.16)$$

$$m = \sqrt{\frac{27}{2} \frac{\sigma_c - \sigma_t}{\sigma_c + \sigma_t}} \quad (2.17)$$

This approach is used in order to introduce the tensocompression asymmetry observed in SMA, and in this way, the material is modeled as isotropic with a Prager - Lode type limit function.

2.3.3 Time-discrete model and solution algorithm

The entire model consists in a non-linear equation system, treated by Auricchio and Petrini [19] as an implicit time-discrete strain-driven problem. The convention, for sake of notation simplicity establishes the pedix n for all the variables evaluated at $t = t_{n+1}$.

Known the solution at the time t_n and the strain tensor at the time t , an implicit backward Euler methods is used to integrate the model rate equations; the stress history is then derived from the strain history by means of a procedure known as return-map [20]. Using this integration scheme, the discrete framework is structured as follows

$$\left\{ \begin{array}{l} p = K[\theta - 3\alpha(T - T_0)] \\ \mathbf{s} = 2G(\mathbf{e} - \mathbf{e}^{tr}) \\ \mathbf{X} = \mathbf{s} - \beta\langle T - T^* \rangle \frac{\mathbf{e}^{tr}}{\|\mathbf{e}^{tr}\|} - h\mathbf{e}^{tr} - \gamma \frac{\mathbf{e}^{tr}}{\|\mathbf{e}^{tr}\|} \\ \gamma \geq 0 \\ \mathbf{e}^{tr} = \mathbf{e}_n^{tr} + \Delta\zeta \frac{\mathbf{X}}{\|\mathbf{X}\|} \\ \|\mathbf{e}^{tr}\| \leq \varepsilon_L \\ F(\mathbf{X}) = \|\mathbf{X}\| - R \leq 0 \\ \Delta\zeta \geq 0, \quad \Delta\zeta F(\mathbf{X}) = 0 \end{array} \right. \quad (2.18)$$

The return-map scheme belongs to a family of elastic-predictor plastic-corrector, consisting in two stages. Into the first one, who belongs to the elastic predictor, a purely elastic *trial state* is computed; in the second one, if the trial state violates the constitutive conditions, a *inelastic correction* is computed using the trial state as initial condition. For this model, the trial state is evaluated for “frozen” internal variables. A trial limit function is computed and compared with the condition described in eq.2.9. If such a condition is violated, the step is considered inelastic and the evolution equations need to be integrated.

To treat an inelastic step, the problem is formulated in residual form, in order to solve the non linear equation system with a Newton-Raphson method. It is important to note that an inelastic state could be related to an unsaturated or a saturated condition, and the discrete model has also to be able to distinguish them with a proper procedure. The procedure starts with the assumption of $\|\mathbf{e}^{tr}\| < \varepsilon_L$, which implies $\gamma = 0$, and consists in an unsaturated condition. The system in this case becomes:

$$\begin{aligned} \mathbf{R}^X &= \mathbf{X} - \mathbf{s}^{TR} + \beta \langle T - T^* \rangle \frac{\partial \|\mathbf{e}^{tr}\|}{\partial \mathbf{e}^{tr}} + h \mathbf{e}^{tr}, \\ R^{\Delta\zeta} &= \|\mathbf{X}\| - R = 0. \end{aligned} \quad (2.19)$$

It is possible now to solve the seven non-linear scalar equations with a Newton-Raphson method to find the seven scalar unknowns, (six components of \mathbf{X} and $\Delta\zeta$). At this point, the solution is checked to evaluate its admissibility. If the solution is not admissible (i.e., $\|\mathbf{e}^{tr}\| > \varepsilon_L$), the state consists in a saturated condition (i.e., $\|\mathbf{e}^{tr}\| = \varepsilon_L$), which implies $\gamma > 0$, and the system in residual form becomes:

$$\begin{aligned} \mathbf{R}^X &= \mathbf{X} - \mathbf{s}^{TR} + \beta \langle T - T^* \rangle \frac{\partial \|\mathbf{e}^{tr}\|}{\partial \mathbf{e}^{tr}} + h \mathbf{e}^{tr} + \gamma \frac{\mathbf{e}^{tr}}{\|\mathbf{e}^{tr}\|}, \\ R^{\Delta\zeta} &= \|\mathbf{X}\| - R = 0, \\ R^\gamma &= \|\mathbf{e}^{tr}\| - \varepsilon_L = 0. \end{aligned} \quad (2.20)$$

In this case, the Newton-Raphson method is used to find eight unknowns, constituted by the six components of \mathbf{X} , $\Delta\zeta$, and γ (for the details about the form of the tangent matrix please refer to [19]).

2.3.4 Model parameters

After the model definition, the material parameters need to be extrapolated by the experimental data with a process called calibrations. Auricchio et al. [31] defined a simple methodology to calibrate the parameter for Souza model. The experimental data is based on the comparison between two thermal cycling tests at constant stress (figure 2.2).

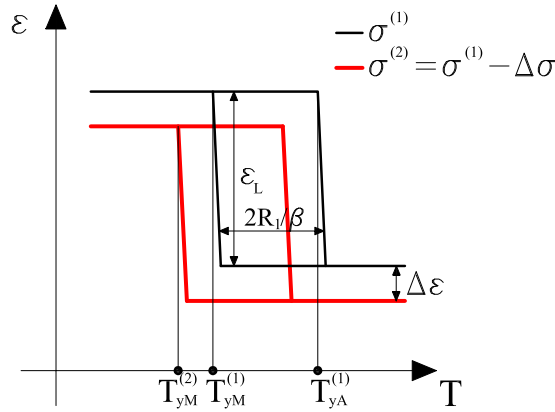


Figure 2.2: Two strain-temperature curves at two constant stresses $\sigma^{(1)} > \sigma^{(2)}$. [32]

The identification of ε_L is trivial and corresponds to the strain associated to the plateau phase in the diagram. E and β are defined, respectively, as $\frac{\partial \sigma}{\partial \varepsilon}$ and $\frac{\partial \sigma}{\partial T}$ (see figure 2.3).

These parameters can be identified starting from fig.2.2 defining $\Delta T = T_{yM}^{(1)} - T_{yM}^{(2)}$ and $\Delta \sigma = \sigma^{(1)} - \sigma^{(2)}$. The elastic radius parameter R can be derived in two ways, depending from the experimental data and the characteristic of limit function. In fact, classic Souza model uses eq. 2.9 as limit function, and the elastic radius can be derived subtracting the two relations

$$\begin{cases} \sigma - \beta(T_{yM} - T^*) = R, \\ \sigma - \beta(T_{yA} - T^*) = -R. \end{cases} \quad (2.21)$$

On the other way, if Auricchio and Petrini improvements are imple-

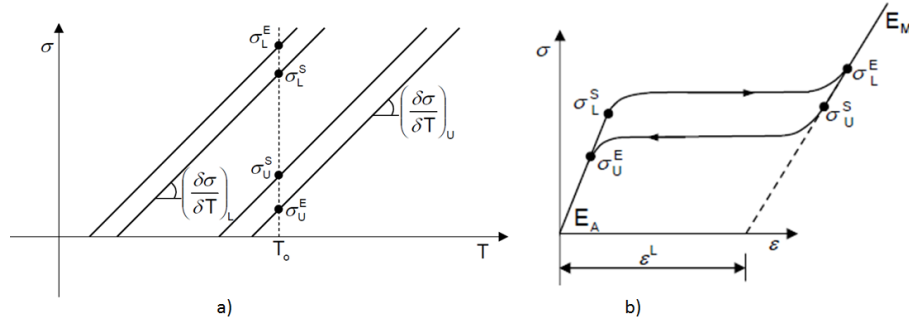


Figure 2.3: a) stress-temperature curve, b) stress-strain curve. Both the curve highlight the physical meaning of some material parameters

mented, the elastic radius can be calculated with eq.2.16. The Abaqus subroutine who implements the model improvements, accepting as material parameters the critical stress or, if available, directly R and m . Concerning to hardening parameter h , starting from $\frac{\partial \sigma}{\partial \epsilon} = \frac{Eh}{E+h}$ and considering the dependence of the stress on temperature $\left(\frac{\partial \sigma}{\partial \epsilon} = \frac{\partial \sigma}{\partial T} \frac{\partial T}{\partial \epsilon} = \beta \frac{\partial T}{\partial \epsilon} \right)$, with simple computations it can be found that

$$h = \left(\frac{1}{\beta} \frac{\partial \epsilon}{\partial T} - \frac{1}{E} \right)^{-1} \quad (2.22)$$

Finally, to compute T^* , the following expression, directly derived from $\sigma^{(1)} - \beta(T_{yM}^{(1)} - T^*) = R$, can be used

$$T^* = T_{yM}^{(1)} + \frac{R - \sigma^{(1)}}{\beta}.$$

Consequently, table 2.1 with the material parameter adopted in this work, derived from [19] is shown.

Table 2.1: Material parameters.

| | | |
|-----------------|---------------------------------------|------------------|
| E | Elastic moduli | 53000 MPa |
| ν | Poisson's ratio | 0.33 |
| h | Linear hardening parameter | 1000 MPa |
| β | Stress-temperature relation parameter | 2.1 MPa/K |
| T^* | Reference temperature | 245 K |
| σ_c | Critical traction stress | 72 MPa |
| σ_t | Critical compression stress | 56 MPa |
| ε_L | Maximum trasformation strain norm | 4.0 % |
| M_f | Martensite finish temperature | 223 K |
| M_s | Martensite starting temperature | 239 K |
| A_f | Austenite finish temperature | 260 K |
| A_s | Austenite starting temperarut | 2248 K |
| α | Thermal exapnsion coefficient | $10^{-6} K^{-1}$ |
| δ | Regularized norm coefficient | 0.02 |

2.3.5 Considerations about Souza model

This 3D phenomenological model, is able to describe accurately the primary effects related to SMAs, and shows many advantages. Despite the use of only one second-order tensor as internal variable allows only to distinguish between a generic parent phase and a generic product phase, the model is able to reproduce martensite reorientation process, but in an approximated way. Another big advantage is the thermodynamic consistency, verified by the satisfaction of the second law of thermodynamics in the form of the Clausius-Duhem inequality (see [19] for details). On the other hand the model shows some disadvantages. First, as mentioned previously, the model structure allows only to distinguish between a generic parent phase and a generic product phase. More precisely, the model is not able to distinguish between austenite and twinned martensite, both characterized by the ab-

sence of an associated macroscopic strain. For the same reason, the model is not able to provide a physical description of the phenomenon called martensite reorientation. Moreover the model is not able to catch some of the secondary effects typical for SMA, such as the difference of elastic properties observed between austenite and martensite. Moreover the model is theoretically founded on the small-strain regime assumption, with all the limitations that this approach gives (a finite-strain formulation is described in [15]).

2.3.6 Stress-strain examples

Auricchio and Petrini [19] tested the model with several test both uniaxial and bi-axial under strain, stress or temperature control. The uniaxial tests (fig.2.4) showed the capability of the model to predict both PE and SME (when $T < A_f$), in addition with an asymmetric behavior in tension and compression (eq. 2.16).

2.4 Lagoudas phenomenological model

Lagoudas et al. [22] proposed in 1996 a 3-D phenomenological model, able to unify three different SMA models. The authors chose the Cauchy stress tensor σ and the temperature T as control variables, and the transformation strain tensor ε^{tr} and the martensite fraction ζ as internal variables. As thermodynamical potential total Gibbs free energy, G , was used. For a polycrystalline SMA, assuming linear thermoelastic response and non-linear transformation-hardening behaviour, G is given by

$$G(\sigma, T, \zeta, \varepsilon^{tr}) = \frac{11}{2\rho} \sigma : S : \sigma - \frac{1}{\rho} \sigma : [\alpha(T - T_0) + \varepsilon^{tr}] + c[(T - T_0) - T \ln \frac{T}{T_0}] - s_0 T + u_0 + f(\zeta) \quad (2.23)$$

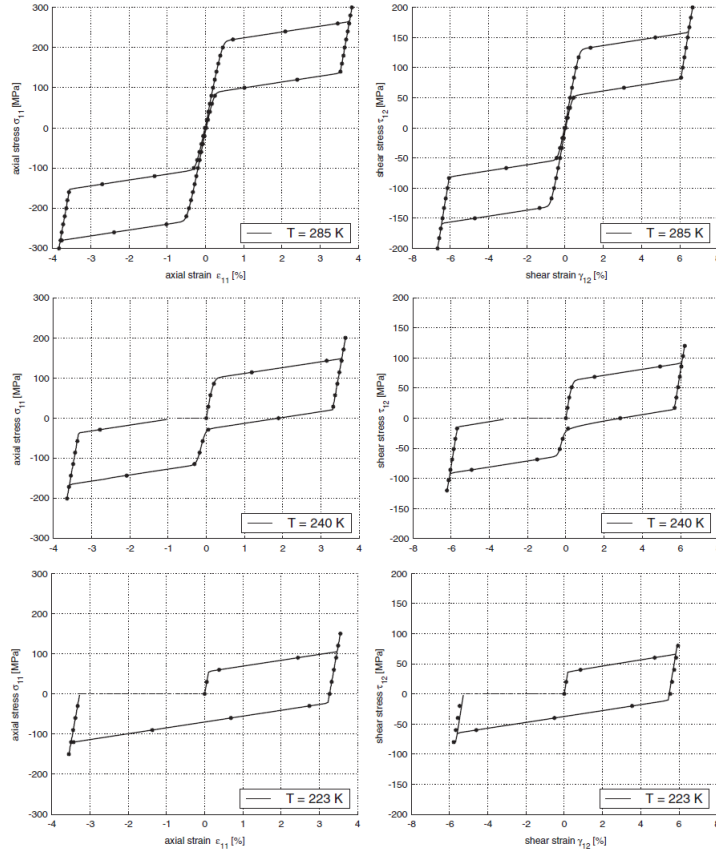


Figure 2.4: Tension-compression tests (left part) and torsion tests (right part) under stress control with continuous line: $T = 285$ K (upper); $T = 240$ K (centre); $T = 223$ K (lower). For $T < A_s = 248$ K strain recovery induced by a heating cycle is indicated with a dash-dot line. Stress increment per step during tension-compression tests: 3 MPa (continuous line) and 30 MPa (dot line). Stress increment per step during torsion tests: 2 MPa (continuous line) and 20 MPa (dot line) [19]

where the pedix 0 in T_0 indicates the reference state. The material parameters S , α , ρ , c , s_0 and u_0 are, respectively, the effective compliance tensor, effective thermal expansion coefficient tensor, density, effective specific heat, effective specific entropy and effective specific internal energy. The

term “effective” indicates that all those material properties are defined in terms of the martensite volume fraction ζ by the rule of mixtures. If A is the material property defined in martensite (M) and austenite (A), the effective parameter is

$$A = A^A + \zeta(A^M - A^A) \quad (2.24)$$

$f(\zeta)$ corresponds to the transformation hardening function and, with this implementation, is possible to change its functional form, in order to follow three different SMA model. In particular, the models are:

- Exponential model (Tanaka et al. [30])
- Cosine model (Liang and Rogers [24])
- Polynomial model (Boyd and Lagoudas [22])

As seen in section 1.3.1 , eq. 2.23 is derived in order to define the following constitutive relations:

$$\varepsilon = \mathbf{S} : \sigma + \alpha(T - T_0)i\varepsilon^t. \quad (2.25)$$

$$\pi = \sigma : \mathbf{\Lambda} + \frac{1}{2}\sigma : \mathbf{\Delta S} : \sigma + \sigma(T - T_0) - \rho\Delta c[(T - T_0) - T \ln \frac{T}{T_0}] + \rho\Delta s_0 T - \frac{\partial f}{\partial \zeta} - \rho\Delta u_0 \quad (2.26)$$

where ε is the total strain and π is the thermodynamic force conjugate to ζ (similar to \mathbf{X} in the previous model). The yielding function Φ is defined as follows

$$\begin{cases} \pi - Y^* & \text{if } \zeta < 0 \\ -\pi - Y^* & \text{if } \zeta > 0 \end{cases} \quad (2.27)$$

where Y^* is the measure of internal dissipation due to the phase transformation. The flow rule related to the transformation strain tensor ε^t and the Kuhn-Tucker conditions are expressed as

$$\dot{\varepsilon}^t = \mathbf{\Lambda} \dot{\zeta} \quad (2.28)$$

$$\begin{cases} \dot{\zeta} \geq 0 & \Psi(\sigma, T, \zeta) \leq 0 & \Psi \dot{\zeta} = 0 \\ \dot{\zeta} \leq 0 & \Psi(\sigma, T, \zeta) \leq 0 & \Psi \dot{\zeta} = 0 \end{cases} \quad (2.29)$$

where $\mathbf{\Lambda}$ is called transformation tensor and determines the transformation strain direction. $\mathbf{\Lambda}$ is implemented in this form

$$\begin{cases} \frac{3}{2} H \frac{\sigma'}{\bar{\sigma}}, & \dot{\zeta} > 0 \\ \varepsilon^{t-r} \\ H \frac{\varepsilon^{t-r}}{\bar{\varepsilon}^{t-r}}, \end{cases} \quad (2.30)$$

Where H is the maximum uniaxial transformation strain and $\varepsilon^{(t-)r}$ is the strain at the reversal of the transformation. The authors, integrated the model with backward and forward Euler scheme, solving the constitutive equation system with a Newton-Rapshon method. The mathematical steps have been neglected because are similar to those described in section 2.3.3.

2.4.1 Considerations about Lagoudas model

Lagoudas model needs the following material parameters:

- Austenite and martensite elastic moduli E
- Austenite and martensite thermal expansion coefficient α
- Austenite and martensite start and finish temperatures at zero stress
- Austenite and martensite stress influence coefficients $\rho\Delta s$
- Maximum transformation strain H

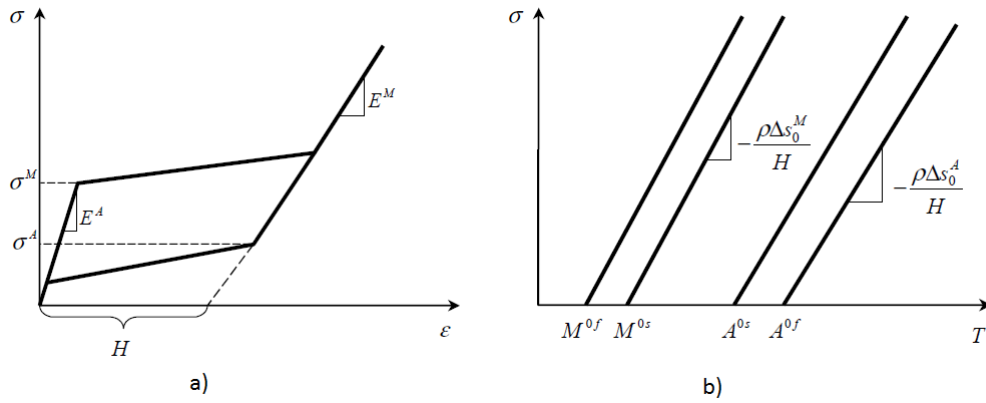


Figure 2.5: a) Schematic of a SMA pseudoelastic test. b) Schematic of a SMA phase diagram.

The model was tested with some simple uniaxial loading cases, at different temperatures, in order to highlight the features caught by the model, and some results are visualized in fig. 2.6. The diagrams show the capability of the model to predict three different SMA hardening functions, as described in section 2.4

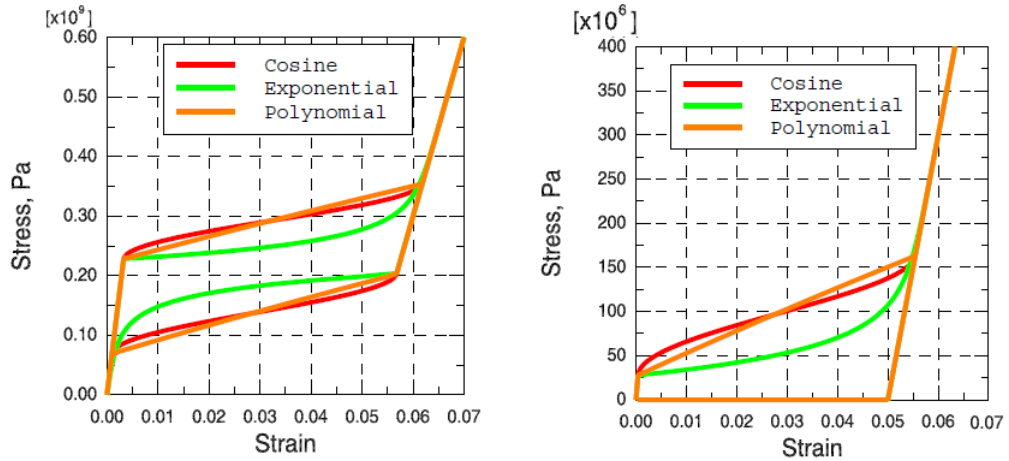


Figure 2.6: a) Loading case to highlight pseudoelastic response of the material. The material is at a temperature higher than the austenitic finish temperature and the loading is applied uniaxially until full transformation is achieved. The material is then unloaded to zero stress, thus recovering all of the transformation strain. b) Loading case demonstrating the Shape Memory Effect material response (SME). Initially the material is at a temperature between the austenitic start and the martensitic start. Uniaxial stress loading is applied, which induces martensitic phase transformation. Upon unloading, the material remains in the martensitic phase and at zero stress there is residual strain. Next, the material is heated to temperature higher than the austenitic finish temperature. During heating, the material undergoes reverse phase transformation and the strain is completely recovered.

Chapter 3

Shape memory alloy VUMAT subroutine implementation

This chapter is focused on the implementation of SMA Souza model (described in chapter 2), in a subroutine suitable for a Finite Element solver (Abaqus 6.10, Abaqus inc., Providence, CA). Abaqus implements different material models in the form of User Subroutines, written in Fortran code, and with different requirements for implicit (UMAT for Abaqus/Standard) and explicit (VUMAT for Abaqus/Explicit) FEA. A pre-existing code, suitable for implicit analyses, has been modified in order to allow the usage for explicit analyses, without changing the code structure. The modified subroutine was tested with a simple Finite Element model, in order to evaluate the capability to predict PE and SME. At the same time, the following subroutines were calibrated (when necessary) and tested with the same model.

- Unmodified Souza code: original UMAT subroutine without modifications, suitable for implicit FEA;
- Lagoudas code: UMAT subroutine that implements the Lagoudas model, described in the previous chapter;

and the results were compared and discussed.

The chapter starts with a brief review of Finite Element Method (FEM), with particular care to difference between implicit and explicit approaches. After that UMAT and VUMAT coding will be described, in order to highlight the different approaches to compute the SMA behavior. At this point the code modifications and tests described previously will be detailed and the results.

3.1 Finite Element Method: a quick overview

The finite element method (FEM) is a *generalized procedure of continuum problems posed by mathematically defined statements* ([33]). It consists on a group of numerical techniques able to compute approximate solutions of partial differential equations as well as of integral equations. In FEM for structural analysis, the system geometry is divided into a number (often large) of discrete elements. These discrete elements are joined by entities called nodes. The set of nodes and finite elements is called the mesh. The number of elements per unit of length or area is called mesh density. In a stress analysis, the nodes displacements are the fundamental variables that a Finite Element solver, like Abaqus, calculates. Once the nodal displacements are known, the stresses and strains in each finite element can be determined easily. Nodal displacements can be obtained following two approaches:

- Implicit method: in this approach, the equilibrium equations need to be solved simultaneously to obtain the displacements of all the nodes. This requirement is best achieved by matrix techniques; therefore, the internal and external force contributions can be written as matrices. This system of equations can then be solved to obtain values of the unknowns nodal displacements. At this point is trivial to find the strain values and ϵ , passing through the constitutive relations, to calculate the stresses in all the elements. It is important to note that implicit

FEM requires to solve the equations system at the end of each solution increment. Moreover, the resolution with an implicit method requires the creation of the global stiffness matrix and its inversion;

- Explicit method: in contrast to implicit methods, an explicit method does not require the simultaneous solving of an equations system or the calculation of a global stiffness matrix. Instead, the solution is advanced kinematically from one increment to the next (for an exhaustive example of problem solving with different approaches see [34]);

The choice between the two approaches can be guided by several reasons. For example, implicit methods result more efficient for solving smooth nonlinear problems; on the other hand, explicit way is the clear choice for a wave propagation analysis. In the middle, there is a wide variety of problems well suited for both the approaches, typically static or quasi-static problems with complex contact issues. For these problems, implicit way shows an absolute stable scheme, but can results in an high number of iterations and computational cost. Concerning to explicit method, they do not require to determine the solution for the whole model at each increment, so the analysis can be more efficient. On the other hand, explicit approach needs particular care for the dynamic control, such as kinetic-internal energy ratio (for quasi-static analyses), that can reduce the time increment and the procedure can be less efficient (see [35] for explicit quasi-static analyses examples). Concerning on the computational cost the explicit method, shows a proportional relationship between computational cost and the number of elements and a roughly inversely proportional relationship with the smallest element dimension. Mesh refinement, therefore, increases the computational cost by increasing the number of elements and reducing the smallest element dimension. For the implicit method, computational cost prediction is more difficult in reason of the problem-dependent relationship between element connectivity and solution cost. Using the implicit method, experience shows

that for many problems the computational cost is roughly proportional to the square of the number of degrees of freedom. The explicit method shows great cost savings over the implicit method as the model size increases, as long as the mesh is relatively uniform. Fig. 3.1 shows a qualitative comparison of cost versus model size (in terms of degrees of freedom) using the explicit and implicit methods. For many models the number of elements is so high that an explicit approach is the only way to get the simulation results in a relatively short time.

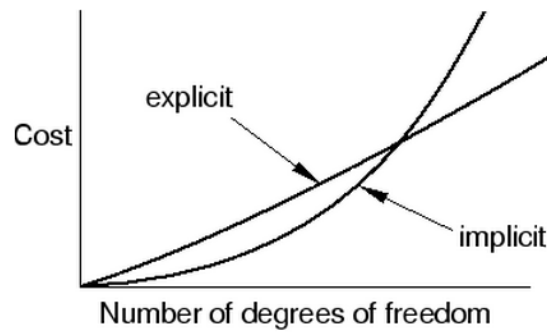


Figure 3.1: Qualitative comparison between implicit and explicit methods in terms of computational cost ([34])

3.2 User material subroutines: UMAT versus VUMAT

In the previous section, the procedure implemented by Finite Element solvers was briefly described. Both implicit and explicit methods need, after the nodal displacement calculation, to introduce the material constitutive relations in order to compute the stresses. Abaqus/Standard and Abaqus/Explicit have interfaces allowing the implementation of general constitutive equations for any material. In particular the user-defined material model can be implemented as user subroutine UMAT (Abaqus/Standard) and VUMAT

(Abaqus/Explicit). These subroutines become necessary when the model for the material of interest is not included in the Abaqus material library.

3.2.1 UMAT subroutine

UMAT constitutive subroutine can be used to define the mechanical constitutive behavior which will be used in implicit analyses. UMAT is called for each material point at each iteration of every increment. The interface implemented in Abaqus/Standard for user-defined materials requires the following variables at the beginning of the increment

- Stress tensor **STRESS(NTENS)**: passed in vectorized form, the stress tensor is updated in the routine in order to be the stress tensor at the end of the increment. The measure of stress used is "true" (Cauchy) stress. The value **NTENS** indicates the array dimension related to the nature of the problem.
- Solution-dependent state variables **STATEV(NSTATEV)**: this array contains the solution-state variables that, as stress, will be updated in the routine. The size of the array is defined by the value **NSTATEV**.
- Temperature **TEMP**: working temperature values
- Predefined field variables
- Increments in temperature (**DTEMP**), strain (**DSTRAN**) and time (**DTIME**)
- User-specified array of material constants associated with the material (**PROPS(NPROPS)**)

The subroutine UMAT has to provide the consistent Jacobian matrix (**DSDDE**), $\frac{\partial \Delta \sigma}{\partial \Delta \varepsilon}$. The Jacobian matrix computation is the key task, because it has demonstrated a direct relationship between accuracy in Jaco-

bian definition and increase in convergence rate. These variables represent the UMAT requirements for a wide variety of problems but, depending on the simulation requirements and/or on material properties, other variables can be requested by the UMAT subroutine, as can be seen in fig. 3.2 (for a detailed description of all the variables see [36]).

```

SUBROUTINE UMAT(STRESS, STATEV, DDSDE, SSE, SPD, SCD, RPL,
1 DDSDDT, DRPLDE, DRPLDT, STRAN, DSTRAN, TIME, DTIME, TEMP, DTEMP,
2 PREDEF, DPRED, CMNAME, NDI, NSHR, NTENS, NSTATV, PROPS, NPROPS,
3 COORDS, DROT, PNEWDT, CELENT, DFGRD0, DFGRD1, NOEL, NPT, LAYER
4 KSPT, KSTEP, KINC)

C
INCLUDE 'ABA_PARAM.INC'
C
CHARACTER*8 CMNAME
C
DIMENSION STRESS(NTENS), STATEV(NSTATV), DDSDE(NTENS, NTENS),
1 DDSDDT(NTENS), DRPLDE(NTENS), STRAN(NTENS), DSTRAN(NTENS),
2 PREDEF(1), DPRED(1), PROPS(NPROPS), COORDS(3), DROT(3, 3),
3 DFGRD0(3, 3), DFGRD1(3, 3)

```

Figure 3.2: UMAT subroutine header.

3.2.2 VUMAT subroutine

As described in the previous sections, VUMAT subroutine is the explicit version of UMAT. This subroutine is called for blocks of material calculation points, which dimension is related to the parameter **nblock**. VUMAT requires the following basic variables

- strain increment **strainInc(nblock, ndir+nshr)**: strain increment tensor, in vectorized form, for each material point (**nblocks** indicates the number of material points, **ndir** and **nshr** the number of direct and shear components, respectively);
- **stressOld(nblock, ndir+nshr)**: stress tensor, in vectorized form, at the beginning of the increment;

- **stateOld(nblock, nstatev)**: state variables vector evaluated at the beginning of the increment;
- Predefined field variables **fieldOld, fieldNew**
- Thermal properties **tempOld, tempNew** : temperature at the beginning and at the end of the increment;
- Time increment properties : **stepTime** indicates the current time step, **totalTime** is the value of total analysis time and **dt** is the time increment;
- Density **density(nblock)**;

These variables, mixed with a wide variety of other variables in dependence of the typology of the problem (see fig 3.3 for a complete list), are used to update the stress and the state-variables, that will be stored in **stressNew(nblock, ndir+nshr)** and **stateNew(nblock, nstatev)**.

```

      SUBROUTINE VUMAT (
C Read only -
      1  NBLOCK, NDIR, NSHR, NSTATEV, NFIELDV, NPROPS, LANNEAL,
      2  STEPTIME, TOTALTIME, DT, CMNAME, COORDMP, CHARLENGTH,
      3  PROPS, DENSITY, STRAININC, RELSPININC,
      4  TEMPOLD, STRETCHOLD, DEFGRADOLD, FIELDOLD,
      5  STRESSOLD, STATEOLD, ENERINTERNOLD, ENERINELASOLD,
      6  TEMPNEW, STRETCHNEW, DEFGRADNEW, FIELDNEW,
C Write only -
      7  STRESSNEW, STATENEW, ENERINTERNNEW, ENERINELASNEW)
C
      INCLUDE 'VABA_PARAM.INC'
C

```

Figure 3.3: VUMAT subroutine header.

3.2.3 Comparison between VUMAT and UMAT

There is a number of significant differences between the UMAT and VUMAT interfaces. For example, VUMAT uses a two-state architecture: the initial values are in the OLD arrays, the new values must be put in the NEW arrays. VUMAT subroutines do not need the definition of Jacobian matrix, in reason of the explicit approach described in section 3.1. For the same reason, while UMAT are called for each material point at every time increment, VUMAT subroutines are called only for small block of material points, making the subroutine call consistent with the explicit method structure, where is not required to satisfy the equilibrium relations for the whole model at every time increment. The different variables must be in vectorized form, instead of UMAT where this is not mandatory. Concerning to the requirements about the variables, VUMAT subroutines do not need the strain at the beginning of the increment, because the stress at the end of the increment is derived as the sum of the stress tensor at the beginning of the increment and the constitutive relations evaluated for the strain increment.

3.3 SMA VUMAT implementation.

Resuming the previous sections, it is clear that:

- For FEM models with an high number of elements, explicit approach results more efficient;
- UMAT and VUMAT subroutines show different coding structure, and this conclusion does not allow to switch from one to another directly;

Moreover, for many models UMAT coding results more natural than VUMAT coding, because, many authors (i.e. [19], [22]) used a Backward Euler Scheme to get the discrete framework of the model, in order to avoid stability problems. For these reasons, a computational approach able to switch

between UMAT and VUMAT without distort the code structure could be interesting. In this way is possible to investigate the advantages (or disadvantages, as well) by mixing the efficiency of explicit methods with the natural aptitude of UMAT coding.

As introduced at the beginning of the chapter, a UMAT subroutine implementing the Souza model ([19]), coded in Fortran language, was available for testing this new approach. Starting from the assumption that FEM integration with different methods (implicit and explicit) is completely disconnected from discrete framework integration of user-material subroutine, is possible to create a control code able to convert the variables requirements of a UMAT interface into a set of variables suitable for a VUMAT interface. This code needs to take in account not only the different variables, but also the different structural requirements (sec.3.2.3), such as the need of vectorization and the difference in subroutine calls. Resuming the eq. 2.5, the following relation represents the key to switch the variables.

$$\mathbf{s} = \frac{\partial \Psi}{\partial \mathbf{e}} = 2G(\mathbf{e} - \mathbf{e}^{tr}) \quad (3.1)$$

This relation, passing into the discrete framework implemented in the UMAT subroutine, will be

$$\mathbf{s}_{\text{new}} = \frac{\partial \Psi}{\partial \mathbf{e}} = 2G(\mathbf{e}_{\text{new}} - \mathbf{e}_{\text{new}}^{tr}) \quad (3.2)$$

where $\mathbf{e}_{\text{new}} = \mathbf{e}_{\text{old}} + \Delta \mathbf{e}$ and $\mathbf{e}_{\text{new}}^{tr} = \mathbf{e}_{\text{old}}^{tr}$ for a elastic trial state, and, if the step is inelastic, is calculated with the procedure described in sec.2.3.3 . The apex "new" indicates a variable evaluated at the beginning of the increment, while the apex "old" is for a variable at the end of the increment. This relation will be translated in the Fortran code as:

```

do i = 1 : NTENS
STRESS(i) = 2G(STRAN(i) + DSTRAN(i) - STATEV(i))   (3.3)
end do

```

Where G is the shear modulus. Resuming section 3.2 can be easily seen that all the variables included in this relation can be found directly in VUMAT requirements, except the strain evaluated at the beginning of the increment. For this reason, the control code for the switch between UMAT and VUMAT contained the relations that, starting from variables available for VUMAT (in particular **stressOld**), extrapolate the strain value at the beginning of the increment. The code is structured as follow

- Starting from **stressOld** the deviatoric (**esse**) and volumetric (**p**) part of the stress at the beginning of the increment are calculated as

```

do j = 1 : nblock
    do i = 1, 3
        esse(j, i) = stressOld(j, i) - trace(j)/3
    end do
    do i = 4, 6
        esse(j, i) = stressOld(j, i)
    end do
    p(j) = trace(j)/three
end do

```

(3.4)

- Using eq.3.2, and remembering the assumption that transformation strain ε_{tr} gives only deviatoric contributions, the strain at the beginning of the increment will be

```

do j = 1 : nblock
  do i = 1, 6
    eOld(j, i) = stateOld(j, i) + esse(j, i)/gg2
  end do
  theta(j) = p(j)/3BK          do i = 1, 3
    strainOld(j, i) = eOld(j, i) + theta(j)      (3.5)
  end do
  do i = 4, 6
    strainOld(j, i) = eOld(j, i)
  end do
end do

```

Where BK is the bulk modulus. It is important to note the iterations around **nblock**, reasoned by the need, in VUMAT, to call the subroutine for nblock material points. This control code, mixed with state-variable assingement in the proper array **stateOld**, should allow the usage of the UMAT Souza code for explicit analyses.

3.4 SMA VUMAT tests

To show the VUMAT capability to predict the main features of SMA materials in the following sections, several uniaxial stressstrain processes under strain and stress control will be described. In particular, the first test is a strain-driven test able to emphasize PE and the linear relationship between stress and temperature. The second one is a stress-driven test, structured in order to highlight SME with changes in temperature.

3.4.1 Pseudoelasticity test

A three-dimensional unit cube ($1\text{mm} \times 1\text{mm} \times 1\text{mm}$) is subjected to uniaxial loading-unloading cycle, both in tension and compression at different temperatures (always $T > A_f$, in order to emphasize PE). The cube consists on a single finite element, as shown in fig. 3.5. The elements used in these tests are eight-node brick element with reduced integration C3D8R. The cube is constrained with the proper boundary conditions (BCs), with symmetry conditions correlated with a uniaxial loading test. Nodal temperatures are kept constant during the analysis, and the test was performed at three different temperature (285 K, 300 K, 310 K) in order to highlight the stress-temperature linear relationship. The material parameters are the same proposed by Auricchio and Petrini [19] and are showed in table.3.1

Table 3.1: Material parameters.

| | | |
|-----------------|---------------------------------------|------------------|
| E | Elastic moduli | 53000 MPa |
| ν | Poisson's ratio | 0.33 |
| h | Linear hardening parameter | 1000 MPa |
| β | Stress-temperature relation parameter | 2.1 MPa/K |
| T^* | Reference temperature | 245 K |
| σ_c | Critical traction stress | 72 MPa |
| σ_t | Critical compression stress | 56 MPa |
| ε_L | Maximum trasformation strain norm | 4.0 % |
| M_f | Martensite finish temperature | 223 K |
| M_s | Martensite starting temperature | 239 K |
| A_f | Austenite finish temperature | 260 K |
| A_s | Austenite starting temperarut | 2248 K |
| α | Thermal exapnsion coefficient | $10^{-6} K^{-1}$ |
| δ | Regularized norm coefficient | 0.02 |

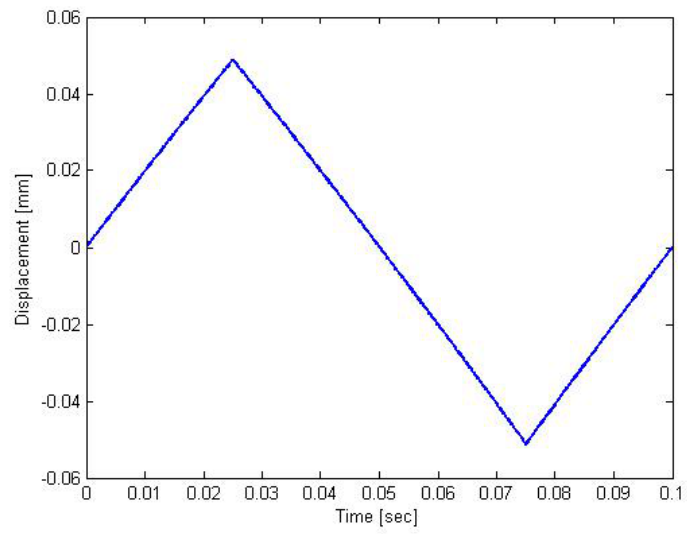


Figure 3.4: Displacement profile along z axis imposed during PE test.

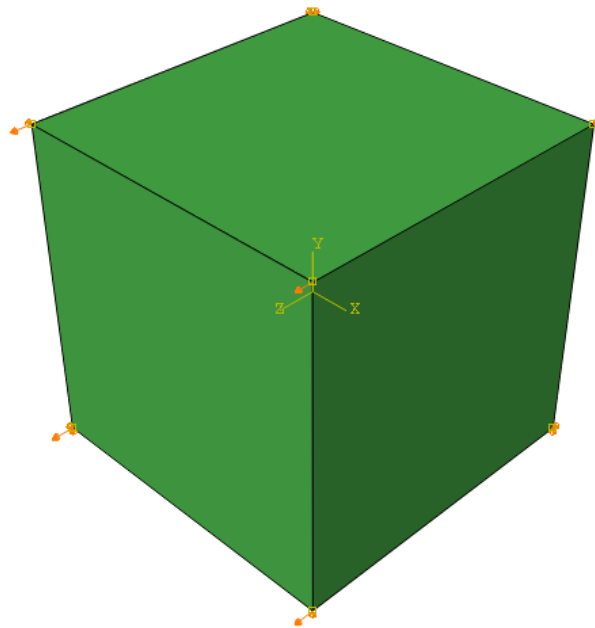


Figure 3.5: FEA part for uniaxial tests.

This test is composed by the following steps

- Step 1: displacement of 0.05 mm along z direction in the nodes corresponding to the free face of the cube;
- Step 2: release of the displacement condition in order to let strain recovery happens;
- Step 3: equal to step 1 but with a displacement of -0.04 mm along z direction;
- Step 4: equal to step 2;

3.4.2 Shape Memory Effect test

The same FEM model (part+ BCs) has been used to perform another test, structured in order to highlight the capability of the subroutine to catch the SME behavior. The simulation is stress-driven and the nodal temperature varies during the simulation, in order to activate the SME. Initial temperature is fixed at the value of 210 K $< M_f$, so that after a loading-unloading cycle, a residual strain is clearly visible. After that the temperature is raised to the value of 320 K $> A_f$, recovering, in this way, all the residual strain. This test is composed by the following steps (illustrated in fig.3.6)

- Step 1: application of a loading-unloading cycle along z direction in the nodes corresponding the free face of the cube. The loading history is triangular and the maximum value corresponds to a value of 120 N;
- Step 2: after the loading removal is possible to see a residual strain;
- Step 3: the temperature is raised from the initial value of 210 K ,with a triangular-shaped history with a maximum value of 320 K;

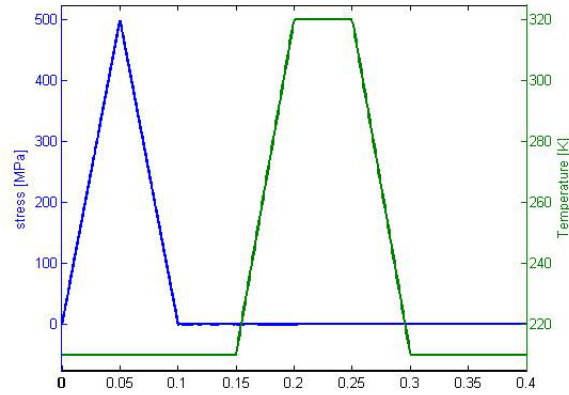


Figure 3.6: Stress and temperature profiles imposed during SME test.

3.5 Results and comparison

In this section the results obtained by the two tests will be described. In order to validate the subroutine quality, the same tests were performed implementing other subroutines and the associated results were compared. In particular, the first comparison is between the SMA_VUMAT and the original UMAT code, in order to demonstrate the basic assumption of independency between Finite Element integration scheme and constitutive relations integration scheme. The second comparison is between the SMA_VUMAT and the SMA_UM, based on Lagoudas model ([22]), in order to validate the results, obtained with the new approach, with a robust and tested algorithm.

3.5.1 Results discussion

The results of PE tests are shown in fig. 3.7. The stress-strain diagram shows the typical SMA behaviors, with yielding values correlated to the results obtained Auricchio and Petrini ([19]). The changes in temperatures highlight the linear relationship between stress and temperature.

It is important to note that, in a neighbourhood of zero, a small residual strain has not been recovered (see fig.3.8). This is due to the regularized norm

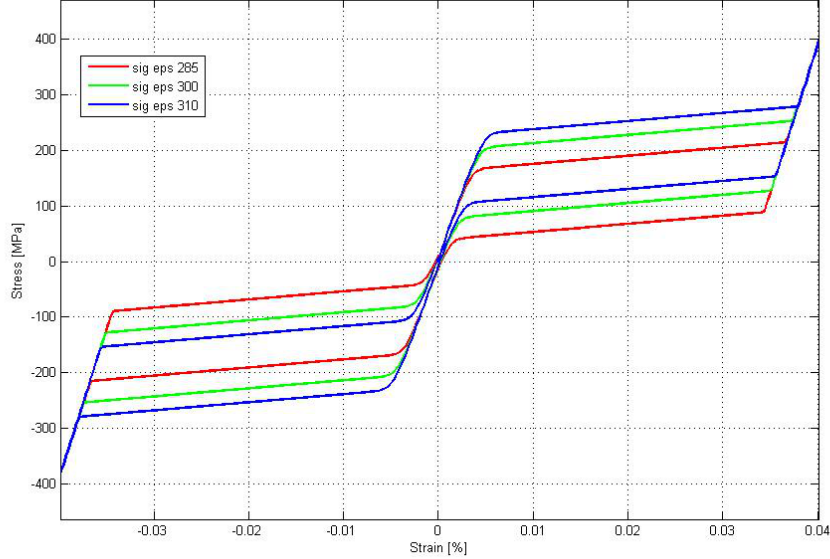


Figure 3.7: SMA_VUMAT tension-compression tests at different temperatures.

definition mentioned in section 2.3.2, which allows to evaluate the transformation strain norm derivative also when $\|\mathbf{e}^{tr}\|$ is close to zero without falling into convergence problems. On the other hand, this approach induces the incomplete strain recovery, that shows a residual strain close to the δ value introduced as material parameter. For many applications, this approximation is good, but further convergence analyses should be performed in order to find the optimal δ value.

Concerning to the SME test, the strain history with stress and temperature history, and stress-strain diagram are shown in fig. and fig. , respectively. The strain history (fig.3.9, left) shows the typical SME features, such as the elastic contributions related to the twinned (1) and detwinned (3) martensite, the fast increase related to phase transformation (2) and the residual strain after the load removal (4). Finally, the complete recovery of the strain related to the temperature increase (5) can be observed .

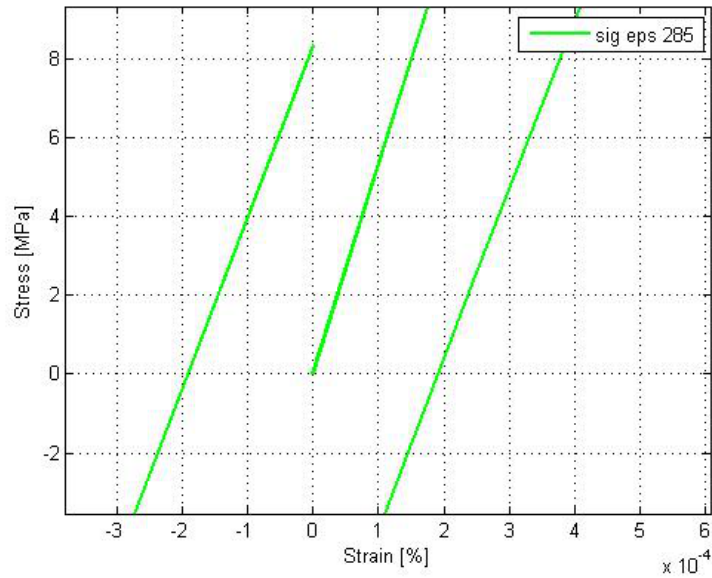


Figure 3.8: PE test at 300 K evaluated in a neighbourhood of 0.

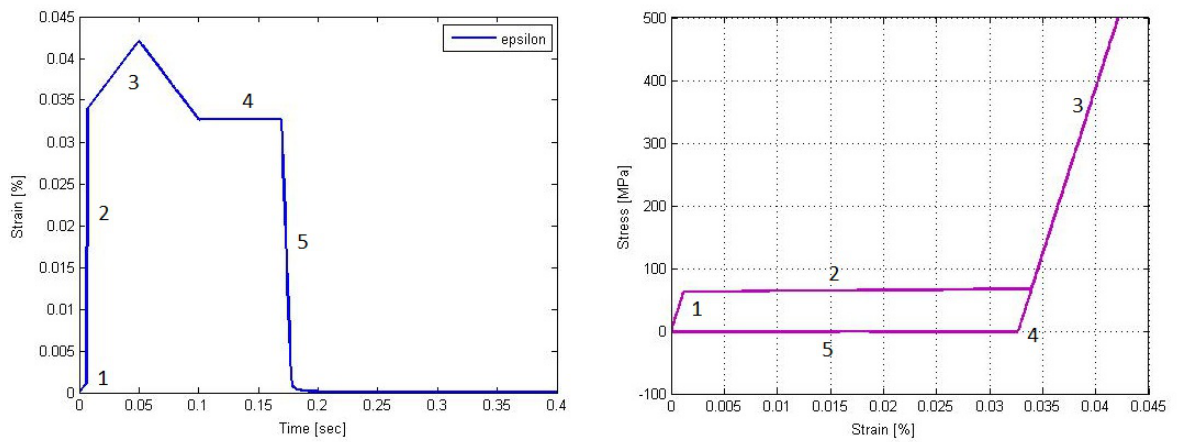


Figure 3.9: SME test results: strain history (*left*), stress-strain diagram (*right*).

3.5.2 Comparison with the UMAT code

This step could be considered trivial at the first sight, but the results are very useful to demonstrate the basic assumption made at the beginning of

this dissertation. In fact this approach has been studied starting from the assumption of complete independence between the integration scheme associated with the Finite Element Method, and the integration scheme related to the constitutive equations. This theoretical assumption allowed the coding of the SMA_VUMAT maintaining an implicit integration scheme. The prove of the quality of this idea consists in the comparison between the SMA_VUMAT (showed in fig.3.10, b and d) and UMAT results (fig.3.10, a and c). The results exhibit a perfect correspondance both in elastic and phase transformation ranges, validating the starting idea.

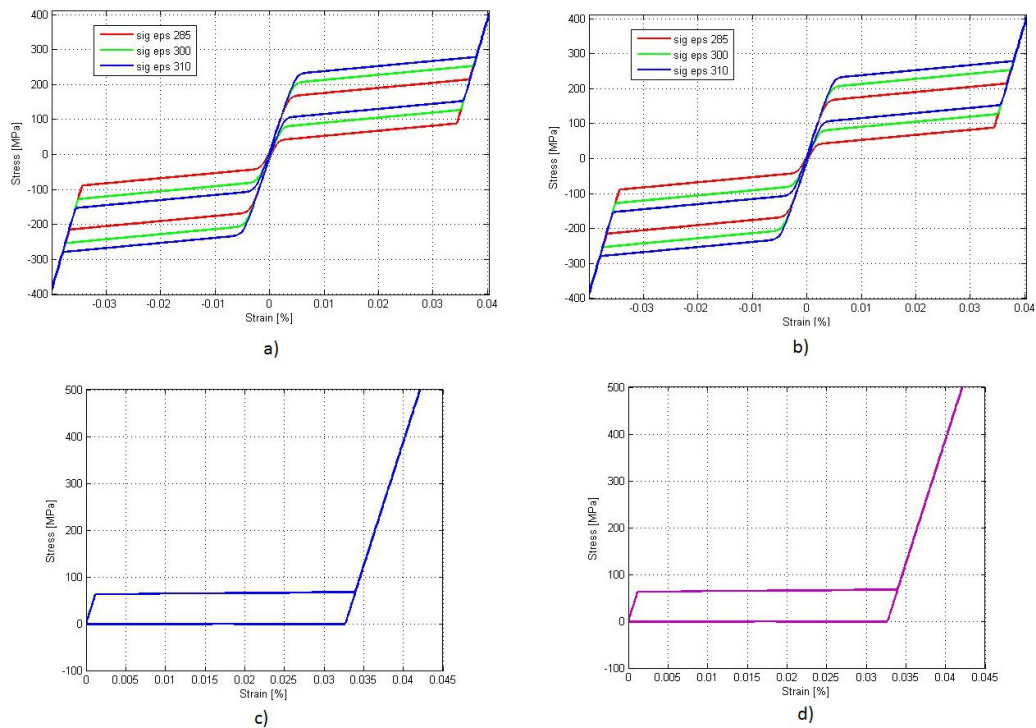


Figure 3.10: SMA_VUMAT versus UMAT: a) and c) are the UMAT results for PE and SME tests, respectively. fig. b) and d) are the SMA_VUMAT results.

3.5.3 Comparison with the SMA_UM

As the previous section looked trivial, this one looks necessary to strongly validate the discrete computational model. In fact, SMA_UM subroutine, an free UMAT subroutine implementing the Lagoudas model ([22]), represents one of the best comparison terms for SMA_VUMAT. Despite the previous section, which does not need to change the parameter setting, in this case parameter requirements for SMA_UM must be studied and calibrated in order to properly compare the results. A resuming table about calibration process is shown in table 3.2

Table 3.2: Material parameters.

| | | |
|------------------|---|------------------------------|
| E^A | Elastic stiffness of the austenite | 53000 MPa |
| E^M | Elastic stiffness of the martensite | 53000 MPa |
| ν | Poisson's ratio | 0.33 |
| α^A | Coefficient of thermal expansion for the austenite | $22.0 \times 10^{-6} K^{-1}$ |
| α^M | Coefficient of thermal expansion for the martensite | $22.0 \times 10^{-6} K^{-1}$ |
| M_f | Martensite finish temperature | 223 K |
| M_s | Martensite starting temperature | 239 K |
| A_f | Austenite finish temperature | 260 K |
| A_s | Austenite starting temperature | 248 K |
| H | Maximum transformation strain | 3.2 |
| $\rho\Delta s^A$ | Stress influence coefficient for austenite | $-0.084 \text{ MPa K}^{-1}$ |
| $\rho\Delta s^M$ | Stress influence coefficient for martensite | $-0.084 \text{ MPa K}^{-1}$ |

These values are directly taken from the material parameter of SMA_VUMAT, when available (E^A , E^M , α^A , α^M and the starting and finish temperatures for austenite and martensite). Other parameters, like H , are related to the parameter ε_L of SMA_VUMAT, but coming out from different ways. More specifically, H is defined as the maximum uniaxial transformation strain, while ε_L is defined as the maximum value of the transformation strain norm

during an uniaxial test. It is possible to manipulate the equations in order to obtain a coefficient able to relate the two parameters. Starting from a simple uniaxial process, the stress tensor will be

$$\sigma = \begin{bmatrix} \sigma & 0 & 0 \\ 0 & 0 & 0 \\ 0 & 0 & 0 \end{bmatrix}$$

and the related deviatoric stress tensor will be

$$\mathbf{s} = \begin{bmatrix} \frac{2}{3} & 0 & 0 \\ 0 & -\frac{1}{3} & 0 \\ 0 & 0 & -\frac{1}{3} \end{bmatrix} \sigma \quad (3.6)$$

resuming the flow rule of Souza model described by equation 2.10 is possible to note that the transformation strain evolution is ruled by the ratio $\mathbf{n} = \frac{\mathbf{s}}{\|\mathbf{s}\|}$. The substitution of eq.3.6 inside that ratio will give

$$\mathbf{n} = \sqrt{\frac{9}{6}} \begin{bmatrix} \frac{2}{3} & 0 & 0 \\ 0 & -\frac{1}{3} & 0 \\ 0 & 0 & -\frac{1}{3} \end{bmatrix} \quad (3.6)$$

and the uniaxial component n_{11} will be

$$n_{11} = \frac{2}{3} \sqrt{\frac{9}{6}} = \sqrt{\frac{2}{3}} \quad (3.6)$$

n_{11} is used in Lagoudas model as reference to find H and, for this reason the coefficient that relates the maximum transformation strain norm and the its uniaxial value, is exactly $\sqrt{\frac{2}{3}}$. For these tests $\varepsilon_L = 0.04$ and the

associated $H = 0.032 = 0.04\sqrt{\frac{2}{3}}$. Concerning to $\rho\Delta s^A$ and $\rho\Delta s^M$, they can be determined from the stress-temperature phase diagram and a pseudoelastic test. More precisely, they are related to the slope of the linear stress-temperature relationship showed by SMA, with the proportional coefficient of $-\frac{1}{H}$ (fig.3.11). The previous definition suggested the direct association between $\rho\Delta s^A$ and $\rho\Delta s^M$ and the SMA_VUMAT parameter β .

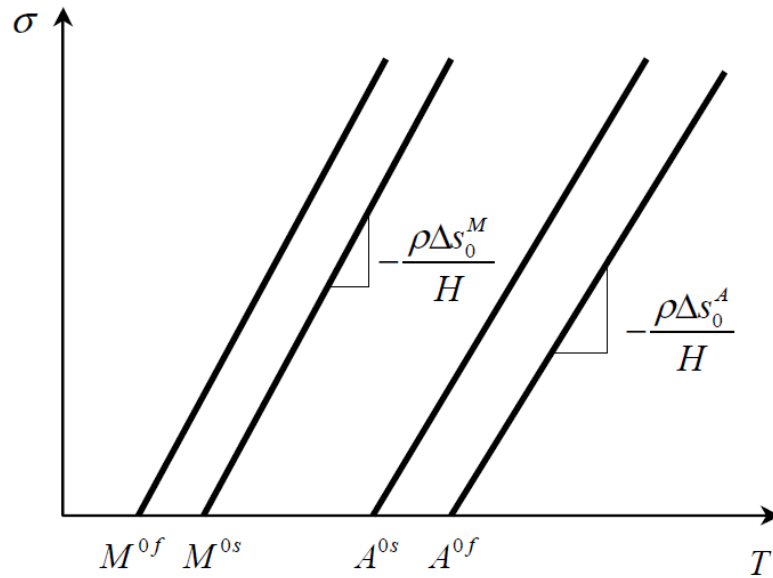


Figure 3.11: Typical SMA stress-temperature phase diagram.

After the parameters calibration, the SMA_UM subroutine has been tested with a PE test at a temperature of 310 K. Lagoudas model was tested using the three different hardening functions (see [22] for details), and the results are illustrated in fig.3.12.

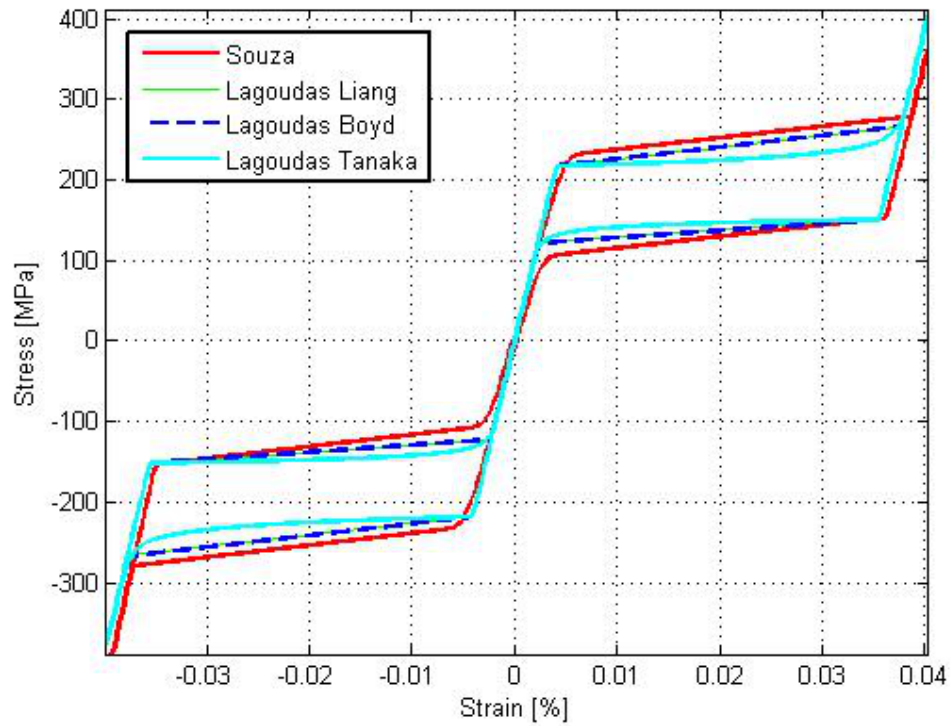


Figure 3.12: Stress-strain diagram computed with SMA_VUMAT and SMA_UM.

The results followed the same pathways and, show similar stress values during the loading-unloading cycle, except for Tanaka hardening rule test

Chapter 4

Realistic examples

The final chapter is focused on the implementation of the SMA_VUMAT subroutine, described and tested in the previous chapters, into two realistic examples. More precisely the first realistic example describes a simple compression test performed on a NiTiNOL carotid stent, an endovascular prosthesis widely-used for the treatment of stenosis in coronary arteries. These devices are driven to the stenosis region and, are deployed with the release of the delivery system constraints. The stent deploys in reason of the PE, that allows the recovery of the plastic strains stored in during the crimping procedure into the delivery system. The example will show the device capability to recover its original shape after a radial compression test The second example describes the behavior of a NiTiNOL microgripper, a microscopic device used to grasp and manipulate microscale objects safely. The functioning principle of the device is based on SME, that allows the thermo-mechanical interaction between the different regions of the micro-gripper in order to achieve the grasping task.

4.1 Pseudo-elastic stent compression example

Cardiovascular diseases (CVD) represent, nowadays, the leading cause of death in Western countries. An estimated 8260000 (>1 in 3) American adults have 1 or more types CVD and such a big prevalence is strongly related with a huge social and economical impact. Among this wide variety of diseases, stroke is the second main cause of death inside CVD, representing the 16.7% of deaths for CVD in United States in 2007. Stroke is defined as the progressive reduction of brain functionality, in response of a decrease of blood flow to the brain. Blood flow can be compromised by a variety of mechanisms, such as embolism from the heart, rupture of an artery (hemorrhage), narrowing and hardening of the arteries leading to the brain. Many of these events can be related to atherosclerosis, defined as a systemic disease process in which fatty deposits, inflammation, cells, and scar tissue build up within the walls of arteries. Individuals who develop atherosclerosis tend to develop it in a number of different types of arteries (large and small arteries and those feeding the heart, brain, kidneys, and extremities), but atherosclerosis of the aorta and its branches and, in particular, stenosis of carotid artery (CA) is one of the causes of stroke. Three main options are available for CA stenosis treatment:

- Carotid endarterectomy (CEA): is a surgical procedure for the correction of carotid stenosis. The procedure consists in the removal of the atheromatous plaque with the opening of the artery. Distal and proximal sides of the artery are clamped and blood flow is directed using a tube in order to cross the clamped region during the procedure;
- Carotid artery stenting (CAS): endovascular, catheter based procedure, with main goal to enlarge the stenotic lumen with the placement of an endovascular prosthesis, with or without the help of an angioplastic balloon. The procedure results minimally invasive, with only one

incision in the femoral artery;

- Medical treatment: pharmacologic therapy based on antiplatelets, anticoagulants and blood-pressure lowering drugs;

The first observation is that medical treatment always associated with CEA or CAS, in order to permit a proper cicatrization (for CEA) and to inhibit organism reactions to the endovascular prosthesis (for CAS). The main goal of therapy is to minimize the risk of stroke or death due to extracranial carotid artery disease. The choice between medical therapy and revascularization should be based upon the assessment of the risk of stroke over time and the risk of stroke due to revascularization itself. The discussion about the decision between medical and revascularization approach is still opened and Bates et al. resumed the huge literature available on this topic summarizing the following conclusions; Medical therapy alone is preferred for patients in whom the risk of revascularization outweighs its benefits, including patients who are at low risk for stroke with medical therapy (symptomatic stenosis less than 50less than 60excessive operator complications. Viceversa it is reasonable to consider revascularization for patients with asymptomatic stenosis greater than 60respectively. Concerning to clinical decision between CEA an CAS the debate is still opened, and the more recent clinical trial, Carotid Revascularization Endarterectomy versus Stent Trial (CREST), did not show an explicit supremacy about the risk of the composite primary outcome of stroke, myocardial infarction, or death. Concerning to deployment procedure, stents can be classified as:

- Balloonexpanding (BX): the prosthesis are mounted on a balloon which is gradually inflated driving the stent deployment
- Self-expanding (SX): SX stents are manufactured at the vessel

diameter, then crimped and constrained in the delivery system; during the deployment the SX stent is gradually released from the catheter recovering the target diameter thanks to its mechanical properties

Typically, stents for CAS belong to self-expanding category and are usually manufactured by, initially, laser-cut procedure of a small diameter tube, and then with different thermo-mechanical treatments in order to induce the activation of the material properties. Besides the deployment mechanism, PE results very important to allow the deformation recovery of the stent, especially in peripheral vessels characterized by tortuous anatomy and significant loading due to the body kinematics. Currently, several peripheral stent designs, with different geometrical and mechanical features are available on the market, feeding new and promising fields of research, but also creating confusion and lack of standardization. FEA has shown to be a very useful tool in the investigation and optimization of stents design, and, as suggested by Auricchio et al. [32], is possible to identify the following issues, which need to be considered in a CAS simulation

- accurate modeling of both peripheral artery and stent design;
- simulation of stent manufacturing process;
- assessment and implementation of stent material properties;
- assessment and implementation of atherosclerotic vessel material properties;
- accurate modeling of stent deployment;
- loading induced by pulsatile blood flow and vessel kinematics.

A complete CAS simulations is beyond the aim of this dissertation and this example will show only the SMA_VUMAT capability to interact

with a more complex model such as a stent portion. As already mentioned in the second chapter, for FEA with a large number of elements explicit approach is kindly suggested and this realistic example falls into this category. Even if the approach is rudely simplified, this simulation shows non-linear geometries and large deformations, including also complex contact issues. The FEM model includes the following parts:

- Stent model: ACCULINK (Abbott, Illinois, USA) stent was chosen for this simulation. The planar design is drawn with a CAD software (Rhinoceros) and the tridimensional surface is imported in Abaqus as a solid part. The mesh is created using a compartmental approach (the main structure is decomposed in many simpler regions, easier to be meshed). At this point the nodal mesh coordinates were sent to a Matlab script coded to roll the planar mesh and to obtain the final model. For this simulations, 40068 linear hexahedral elements of type C3D8R (8-nodes linear brick with reduced integration). The material model implemented for the stent is the SMA_VUMAT;
- Plates: The compression plates model is used to simulate the compression procedure and the subsequent strain recovery step. The plates have been modeled as rigid bodies meshed with 80 three-dimensional, 4-node surface elements with reduced integration (R3D4);

The simulation is composed by two main steps. In the first one the stent is compressed by the relative motion between the two plates. After that, the compression plates return in the original position allowing the strain recovery.

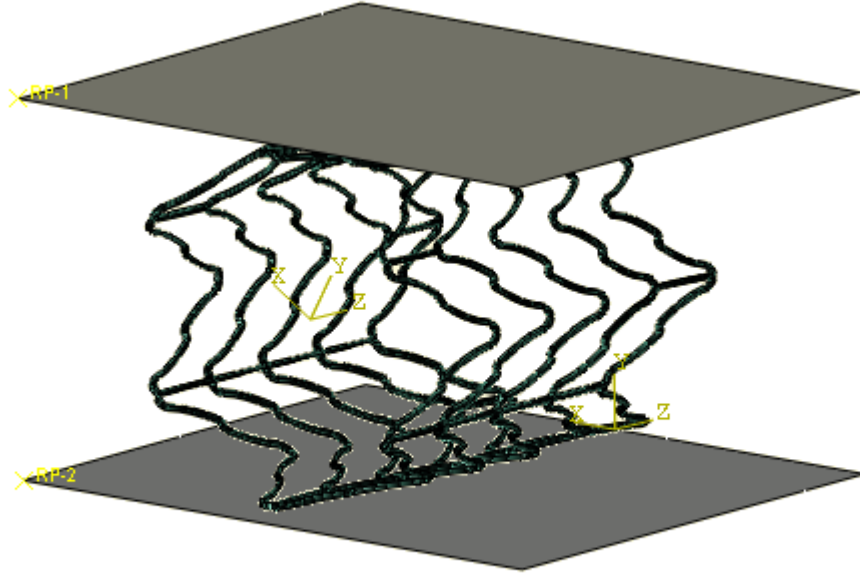


Figure 4.1: FEA stent example viewport.l

4.2 Microgripper example

As described in the introduction, micro-grippers are microscopical actuators able to grasp microscale objects. The geometry of the device analysed is taken from the work of Auricchio et al. [38] and it is shown in fig. 1.6. It is constituted by two parts, the upper part is called as gear actuator, while the lower part is called linear actuator. The device pre-treatment consists in a 2 mm predeformation applied to the linear actuator, while a heating process is applied to the gear actuator. This approach allows to have, at each time, one actuator in the martensitic phase and the other one in austenitic phase.

The microgripper have been modeled with 1840 linear 3D 8-nodes bricks with reduced integration C3D8R. The simulation consists on

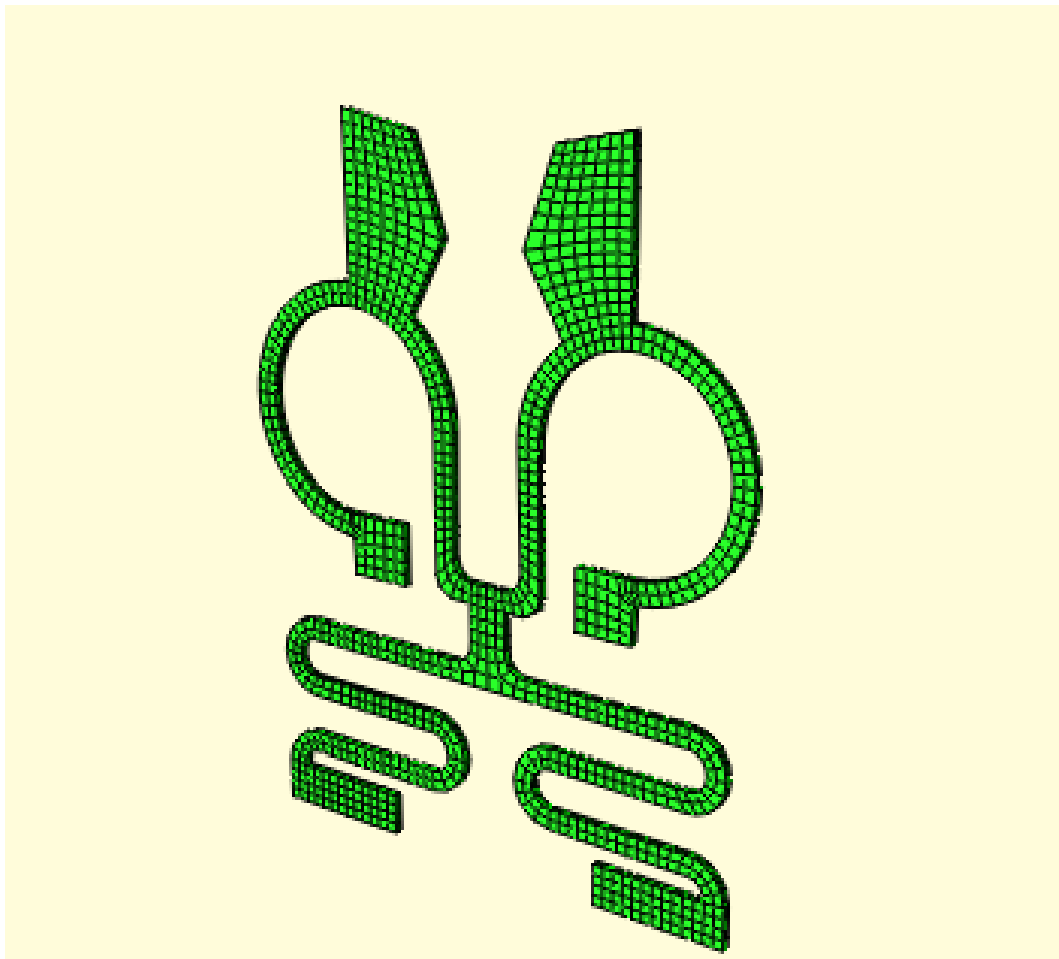


Figure 4.2: Microgripper FEM model.

a series of temperature changes in order to activate the different parts of the device. The linear actuator was heated at a temperature of 30 Celsius degrees, while the gear actuator was cooled at a temperature of -25 Celsius degrees. This combination allows the closure of the gripper. The opposite procedure, with cooling of the linear actuator and heating of the gear actuator allows the gripper opening. The different phases of the simulation are illustrated in fig.

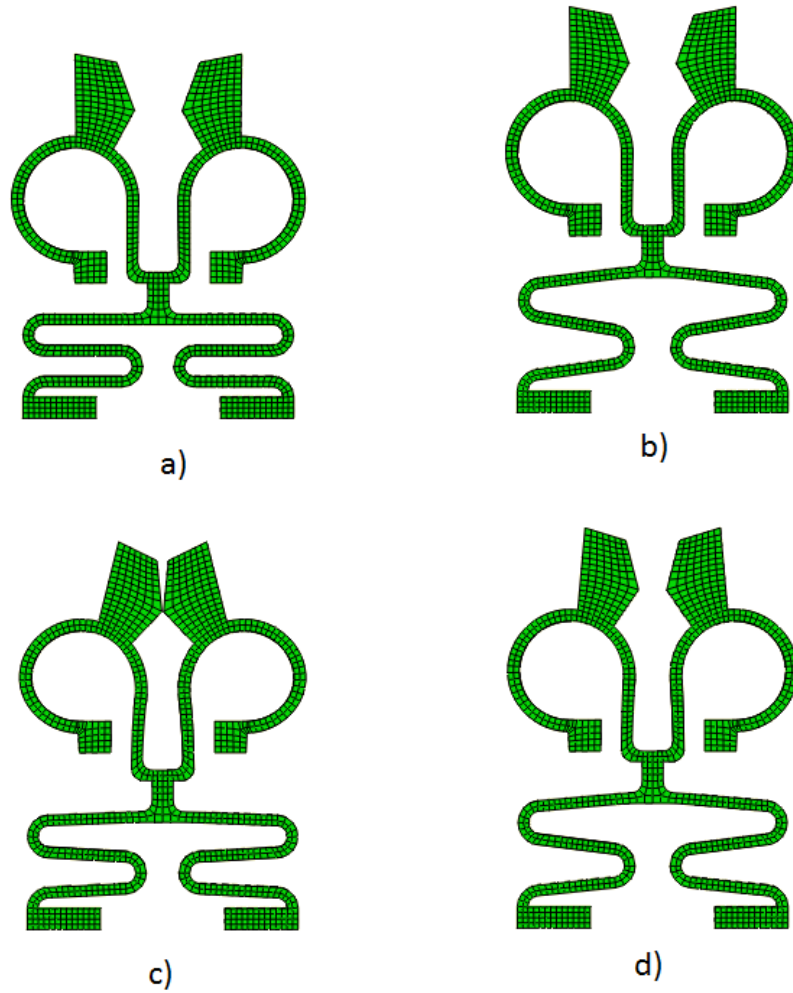


Figure 4.3: Microgripper simulation steps: a) original configuration b) linear actuator memory process c) microgripper closure caused by the heating of the linear actuator and the cooling of the gear actuator d) microgripper opening caused by the heating of the gear actuator and the cooling of the linear actuator.

Conclusions and future works

Shape Memory Alloys (SMA) have been considered as one of the most promising smart materials, thank to the unique ability to recover their initial shape after deformation through a reversible thermo-elastic phase transformation. These features, joined with other attractive properties, such as kink resistance, biocompatibility and fatigue resistance, make SMA an "household" material for many application fields, in particular for medical applications. Vascular application represents one of the most promising fields for SMA material. In particular, devices for minimally invasive procedures, i.e., vascular stents, are often manufactured of SMA material in order to take advantage of the SMA peculiar properties for optimize the intravascular procedure. At the same time, it has been demonstrated that Finite Element Analysis (FEA) can be a valid method to investigate several aspects of stenting procedures, such as the evaluation of interventional technique options or the impact of plaque composition on vessel wall stress. For this reason, a FEA suitable for the simulation of stenting procedure has to take in account a robust and valid SMA constitutive model. In this dissertation, the different topics about SMA constitutive model implementation have been discussed. Starting from the theoretical framework of an attrac-

tive SMA model (Souza model [16]), the main components of a generic SMA constitutive model have been described. After that, the different implementations of SMA model into Abaqus environment have been described, highlighting the differences in coding and structure between implicit and explicit approach, even to simulate the same material. In particular, it has been highlighted the convenience in using an explicit approach for the Finite Element Method integration scheme, while for the constitutive model an implicit approach results often more natural. At this point, the possibility to create a 'bridge' between implicit and explicit approach in order to mix the speed of explicit integration scheme, with the natural coding of implicit approach for constitutive models, has been investigated, starting from the assumption of complete independency between FEM integration scheme and constitutive model. An explicit subroutine (SMA_VUMAT) has been coded starting from an available implicit code, in order to evaluate the capability to create a subroutine able to switch between implicit and explicit approach with few modifications. SMA_VUMAT subroutine has been tested with two simple tests, in order to evaluate the model capability to catch the main SMA feature, that are pseudoelasticity (PE) and shape memory effect (SME). The results showed the capability of the model to catch both the effects precisely without convergence problems. Moreover, a small numerical error is visible in a neighbourhood of the origin, but it is related to a particular improvement introduced by Auricchio and Petrini ([19]) in order to avoid numerical problems in the neighbourhood of $e^{tr} = 0$. To validate the SMA_VUMAT, some comparison have been achieved. The first comparison was between SMA_VUMAT and the original UMAT code. The results showed a perfect association between the data obtained by the tests, validating the basic assumption of independency. The second comparison

was between SMA_VUMAT and SMA_UM developed by Lagoudas et al., that implements the Lagoudas model ([22]). After a step for the parameter calibration, made to evaluate the results starting from the same physical environment, the tests were performed. The curves obtained showed a good association between the different results, even changing the hardening rule in Lagoudas model. After the validation step, in the last chapter, two realistic examples were introduced in order to evaluate, from a qualitative point of view, the SMA_VUMAT capabilities when implemented into more complex models. The results show the good capabilities of the subroutine to catch the SMA features also in more complicated contexts. Consequently the aim of this dissertation has highlighted the different issues of the implementation of user-material subroutines in Abaqus environment. Future works related to this dissertation can be a deep study about the material calibration, and how every material parameter influence the results by a numerical point of view. To improve the SMA_VUMAT, a convergence study about the optimal δ parameter, could be useful. To evaluate the presence of bugs or numerical errors in the code, some biaxial tests could be performed (see [19]). Finally, the update of the model features, with the introduction of tensocompression asymmetry for example, could expand the application field of this attractive computational approach.

Bibliography

- [1] Gandhi, M., Thompson, B. D. Smart materials and structures, Springer,1992
- [2] Schwartz, M. Encyclopedia of smart materials. John Wiley & Sons Inc., 2002
- [3] Duerig T. W., Melton K. N., Stoekel, D. Wayman C.M. Engineering aspects of shape memory alloys, Butterworth-Heinemann, London, 1990
- [4] Buehler, W. J., Gilfrich, J. V., Wiley, R. C., Effects of low-temperature phase changes on the mechanical properties of alloys near composition tini. Journal of Applied Physics 34, 1475 , 1963
- [5] Duerig, T., Pelton, A., Stckel, D. An overview of nitinol medical applications, Materials Science and Engineering A 273-275, 149 - 160,1999
- [6] Shabalovskaya SA. On the nature of the biocompatibility and on medical applications of NiTi shape memory and superelastic alloys. Biomedical Materials and engineering 6(4), 267-89, 1996
- [7] A.R. Peltona, V. Schroeder, M.R. Mitchell, XiaoYan Gong, M. Barney, S.W. Robertson Fatigue and durability of Nitinol stents Journal of the mechanical behavior of biomedical materials 1, 153-164, 2008

- [8] L. Petrini, F. Migliavacca Biomedical applications of Shape Memory Alloys, *Journal of Metallurgy*, vol.2011, Article ID 501483, Accepted in review 8 march 2011
- [9] Van Humbeeck J., Introduction to shape memory alloys, Proceedings of the School and Symposium on Smart Structural Systems Technologies 3-23, 2010
- [10] N.B. Morgan Medical shape memory alloys applications- the market and its products *Materials Science and Engineering*, vol.378 pp.16-23, 2004
- [11] S. Idelsohn, J. Peña, D. Lacroix, A. Planell, F. j. Gil, A. Arcas Continuous mandibular distraction osteogenesis using superelastic shape memory alloy (SMA), *Journal of Material Science*, vol.15, no.4, pp. 541-546, 2004
- [12] L.G. Machado, M.A. Savi, Medical applications of shape memory alloys *Brazilian Journal of Medical and Biological Research*, vol.35, no.6, pp.683-691, 2003
- [13] K. Otsuka, C.M. Wayman Shape memory materials *Cambridge University Press, Cambridge, 1998*
- [14] Lagoudas D. C., *Shape Memory Alloys: Modeling and Engineering Applications*, Springer, 2008
- [15] Jamal Arghavani Thermo-mechanical behavior of shape memory alloys under multiaxial loadings: constitutive modeling and numerical implementation at small and finite strains Sharif University of Technology, Tehran, Iran, Phd thesis in Mechanical Engineering, 2010
- [16] A.C. Souza, E.N. Mamiya, N. Zouain Three-dimensional model for solids undergoing stress-induced phase transformations *European Journal of Mechanics, A: Solids* vol.17 pp.789-806, 1998

- [17] Lubliner J. *Plasticity Theory* Macmillan, New York 1990
- [18] Orgéas L, Favier D. Non-symmetric tension-compression behavior of NiTi alloy. *Journal de Physique IV C8:605 610.*, 1995.
- [19] F. Auricchio, L. Petrini, A three-dimensional model describing stress-temperature induced solid phase transformations. Part I: solution algorithm and boundary value problems, *International Journal for Numerical Methods in Engineering*, vol. 61, pp. 807–836, 2004.
- [20] J.C.Simo, T.J.R. Hughes *Computational Inelasticity* Springer ISBN 0-387-97520-9 1997
- [21] Tanaka K., Nagaki S., A thermomechanical description of materials with internal variables in the process of phase transitions. *Archive of Applied Mechanics* 51 (5), 287-299, 1982
- [22] Boyd J. G., Lagoudas D. C., Thermomechanical response of shape memory composites. *Journal of Intelligent Material Systems and Structures* 5 (3), 333-346., 1994
- [23] Bondaryev E., Wayman C. M., Some stress-strain-temperature relationships for shape memory alloys. *Metallurgical Transaction A* 19A, 2407-2413, 1988
- [24] Liang C., Rogers C. A., One-dimensional thermomechanical constitutive relations for shape memory materials. *Journal of Intelligent Material Systems and Structures* 1 (2), 207-234, 1990
- [25] Brinson, L. C., 1993. One-dimensional constitutive behavior of shape memory alloys: Thermomechanical derivation with non-constant material functions and redefined martensite internal variable. *Journal of Intelligent Material Systems and Structures* 4 (2), 229-242, 1993

- [26] Raniecki B., Lexcellent C., RI-models of pseudoelasticity and their specifications for some shape memory solids. *European Journal of Mechanics - A/Solids* 13, 21-50, 1994
- [27] Leclercq, S., Lexcellent, C., A general macroscopic description of the thermomechanical behavior of shape memory alloys. *Journal of the Mechanics and Physics of Solids* 44 (6), 953-957, 1996
- [28] Qidwai M. A., Lagoudas D. C., On thermomechanics and transformation surfaces of polycrystalline niti shape memory alloy material. *International Journal of Plasticity* 16 (10-11), 1309-1343, 2000
- [29] M. E. Gurtin, *An Introduction to Continuum Mechanics. Mathematics in Science and Engineering vol.158* Academic Press, San Diego,1981.
- [30] Tanaka K., A thermomechanical sketch of shape memory effect: Onedimensional tensile behavior. *Res Mechanica* 18, 251263, 1986
- [31] Auricchio F., Coda A., Reali A., Urbano M., SMA Numerical Modeling versus Experimental Results: Parameter Identification and Model Prediction Capabilities *Journal of Material Engineering and Performanca* vol.18, pp. 649-654, 2009
- [32] Auricchio F., Conti M., Morganti S., Reali A., Shape Memory Alloy: from constitutive modeling to finite element analysis of stent deployment *Computer modeling in engineering and science* vol.18, pp. 649-654, 2009
- [33] O.C. Zienkiewicz, R.L. Taylor *The Finite Element Method* Butterworth Heinemann ISBN 0-7506-5049-4 Fifth edition, Volume 1: The Basis, 2000
- [34] Abaqus 6.10. Getting started with Abaqus: Interactive edition

- [35] Conti M. Finite Element Analysis of Carotid Artery Stenting
Universita' degli Studi di Pavia, Pavia, Italy, phd thesis in Bio-
engineering and Bioinformatics 2010
- [36] Abaqus 6.10. Abaqus User Subroutines Reference Manual, UMAT
section
- [37] G. Sommer, P. Regitnig, L. Koltringer, and G. Holzapfel. Biaxial
mechanical properties of intact and layer-dissected human carotid
arteries at physiological and supraphysiological loadings. *Amer-
ican Journal of Physiology - Heart and Circulatory Physiology*,
298:H898912, 2009
- [38] Auricchio F., Arghavani J., Conti M., Morganti S., Reali A., Ste-
fanelli U. Shape-Memory Alloys: Effective 3D Modeling, Com-
putational Aspects, Analysis of Actuator and Biomedical Devices
Proceedings of ACTUATOR10 - International Conference and Ex-
hibition on New Actuators and Drive Systems 2010

Special thanks

Avevate creduto che avessi scritto tutti i ringraziamenti nell' Acknowledgement? eh eh eh...

Un sospiro e via, i lembi del sipario si chiudono e da un momento all'altro si passa dalla luce del palcoscenico al buio delle quinte. E' stato uno spettacolo lungo anni, estenuante, ma credo ne sia valsa la pena. Faccio un passetto in avanti, scosto il tendone e sono di nuovo sul palco a prendere una marea di fischi o di applausi da parte della eterogenea massa umana che mi trovo davanti. In prima fila c'è tutta la mia famiglia. Sono tutti bellissimi come al solito e, nel mucchio, vedo che i miei genitori e mio fratello mi sorridono come solo loro sanno fare. Quel sorriso mi risveglia qualcosa dentro e, all'improvviso, mi sento completamente rinfrancato da tutte le fatiche e dalle (poche) delusioni di questo lungo periodo. Non potrò mai ringraziarvi abbastanza, siete e resterete i miei pilastri per tutto il resto della mia vita. Spostando lo sguardo sulla destra vedo i ragazzi del laboratorio: Mic, Simone, Fede, Beppe, Carolina, Giulia, Laura, Adrien e tutti gli altri che hanno condiviso con me gioie, problemi e ettoltri di caffè. Siete un gruppo spettacolare e unico, in quanto non ci sono tanti posti dove a così tanta competenza si possa unire tanto calore umano. A proposito di famiglia, nei posti dietro si sente un gran casino e un forte odore di cibo cucinato con piastre elettriche, e , come mi aspettavo, riconosco i

volti dei ragazzi dello Spalla che cucinano roba scongelata (e probabilmente tossica). A tutti voi voglio dire grazie, ma proprio a tutti tutti (si Babuz proprio tutti) perché che sia stata una sbronza, una festa collegiale, una partita di basket, un attacco al Fraccaro o semplicemente un caffè in zona giornali è stato un onore per me condividere il bianco-azzurro e quei quattro muri cadenti con voi. Tra le bestie dello Spalla impossibile non citare i compagni di mille avventure: Leuca, Gnagno, Barbone, Snorky, Slot, Crouch, Niz, Tommaso, Nesti e tanti altri, se non fosse stato per voi questi due anni di fatiche sarebbero stati una noia mortale e spero di continuare a creare aneddoti stupidi con serate pazze e situazioni al limite dell'assurdo come quelle di questi due anni (come uscire alle 4 del pomeriggio e ritornare il giorno dopo a casa, fare un trasloco coatti di divano alle 3 di notte, oppure fare scherzi che non finiscono esattamente come ci si aspettava.... ogni riferimento a mezzi di locomozione altrui è puramente casuale). Nelle vicinanze trovo i ragazzi che mi hanno sopportato in università in questi due anni: Massi, Marcello, Vale, Chiara, Cia, Alberto, Giulia, Stefano, Giusi, Davide, Vito e perdonatemi se mi dimentico qualcuno ma tra un paio d'ore porto la tesi in stampa e devo ancora finire di correggerla XD. Vi ringrazio per aver condiviso con me tante cose in questi due anni e per avermi sempre dimostrato più affetto di quello che, secondo me, merito. Dietro di loro vedo Laura, Roby, Barbara e Sara che discutono se andare in bagno ora o alla fine del secondo atto. Le guardo e sorrido, pensando che, nonostante dei caratteri che stanno agli antipodi, siamo riusciti a convivere piuttosto bene per più di 5 anni e penso che potremo continuare così ancora per molto ;). Più lontano lo sguardo dal palco più i volti si fanno sfocati e irriconoscibili, tuttavia due figure si stagliano dalla massa informe, non fosse altro per l'unicità delle loro sagome. Una sagoma è decisamente lunga e vagamente oristanese,

mentre l'altra é minuscola con una marea di riccioli che volano da una parte all'altra. Vi ringrazio entrambi, perché rappresentate l'ultimo pezzettino che mi é rimasto della parte piú bella del mio periodo a Cagliari e avervi ancora qui dopo tanti anni é una di quelle cose che, al solo pensarci, ti si riempie il cuore. In un palchetto di lato vedo una massa di riccioli castani uscire dal balconcino mentre due persone litigano rumorosamente, una con accento di Busto Arsizio e l'altro con forte accento casertano. Mi metto a ridere come un deficiente e saluto gli amici dell'erasmus: Michela, Monica, Clemente, Albe, Roby, Fiore e tutti gli altri che hanno reso i miei sei mesi a Gent un'esperienza magica e unica nel suo genere. Nel loggione, a distanza considerevole ma stranamente vicina, Zampo, Mario, Buba, Mattia, Marica, Roby, Tore, Erika, Andrea stanno mettendo su tavola per l'ennesima casciana. Vi voglio un bene dell'anima e, anche se non lo dimostro molto bene, siete costantemente nei miei pensieri. Sapere che voi siete li sullo scoglio mi fa da rete di sicurezza nel circo che é diventata la mia vita, e di questo vi ringrazio (non vedo l'ora di tornare a casa per una super-casciana di laurea, E ZU EGUA!). Bene ora che lo spettacolo é finito saluto tutti e torno dietro le quinte per godermi un po di meritato riposo. Mentre mi allontanano i rumori si attenuano e tutto sembra improvvisamente lontano. Mi siedo ed entri tu, bella come sempre. Tutto questo non sarebbe stato cosí bello e fortunato se non ci fossi stata tu, e te lo devo dire dieci, cento, mille volte: GRAZIE amore mio. Grazie di esserci, grazie di starmi vicino e di rendermi una persona migliore ogni giorno, grazie del tuo essere cosí bella e particolare, cosí unica e diversa da tutto quello che vedo intorno a me. Sei la mia pupetta, e io non vedo l'ora di scoprire cosa ci riserva il secondo atto di questo spettacolo, d'altronde lo diceva il buon Freddie Mercury " The show must go on".

Un abbraccio a tutti. Mauro

p.s.: Massi, Marcello e tutti i compagni delle serate Mascule....Finalmente non mi devo più laureare in sociologia!